CALIFORNIA INSTITUTE OF TECHNOLOGY

PASADENA, CALIFORNIA

SM Report 88-7

THREE DIMENSIONAL EFFECTS NEAR A CRACK TIP IN A DUCTILE THREE POINT BEND SPECIMEN PART II: AN EXPERIMENTAL INVESTIGATION USING INTERFEROMETRY AND CAUSTICS

by

Alan T. Zehnder* and Ares J. Rosakis**

Contract N00014-85-K-0596

Graduate Aeronautical Laboratories
California Institute of Technology
Pasadena, California 91125

March 1988

* Present Affiliation: Assistant Professor of Theoretical and Applied Mechanics, Cornell University, Ithaca, New York 14853-1503, Associate Member of ASME.

** Associate Professor of Aeronautics and Applied Mechanics, Division of Engineering and Applied Science, California Institute of Technology, Pasadena, California 91125, Associate Member of ASME.

ABSTRACT

An experimental investigation is undertaken to assess three-dimensional effects near a crack front in a ductile three-point bend specimen. The possibility of using the optical method of caustics for the measurement of the J integral in the presence of large scale yielding and three dimensional fields is also investigated. Experiments using the optical methods of caustics by reflection and Twyman-Green interferometry are performed simultaneously on either side of the test specimen. The load and load-point displacement are also measured. The experimental results are compared with very good agreement to the results of a finite element simulation of the experiment. The caustics experiments are used to obtain a calibration relation between the value of the J integral and the caustic diameter for load levels up to fracture initiation. It is proposed that such a calibration be used in dynamic fracture initiation experiments for the measurement of the time history of the dynamic J-integral.

1. INTRODUCTION

The J integral (Rice, 1968) is commonly used as a measure of a material's fracture toughness in ductile fracture. It is postulated that a stationary, initially sharp, crack will grow when the loads are increased to a level such that a critical value of J is achieved. This critical value is assumed to be a material property. For two-dimensional, monotonically loaded, stationary cracks, the J integral is a path independent line integral evaluated over an open contour surrounding the crack tip, and it is also a measure of the intensity of the crack tip strain singularity (Hutchinson, 1968 and Rice and Rosengren, 1968). For three-dimensional plate specimens containing through cracks, one can define an integral evaluated over a surface surrounding the entire crack front which is equivalent to the two-dimensional J, and for monotonic loading, is independent of the choice of surface. This integral represents an average of the strength of the fields through the thickness. In addition, it can be shown that it represents the average value of the local definition of J along the crack front as given by Shih, Moran and Nakamura, (1986), as discussed on Part I of this investigation (Narasimhan and Rosakis, 1988b).

For either two- or three-dimensional problems, *dynamic* fracture initiation toughness may also be characterized by the J integral. Unfortunately, few proven experimental techniques exist for measuring J under dynamic loading conditions. Existing techniques developed by Costin, Duffy and Freund (1977) and analyzed by Nakamura, Shih and Freund (1985) are based on the use of dynamic boundary value measurements interpreted on the basis of quasistatic J estimation procedures. Because of this limitation, the specimen geometries used in such experiments are highly restricted. As a result, it will

be useful to develop optical methods capable of accurately estimating J directly, regardless of specimen geometry and loading rates. In this paper, the first stages of developing such a technique are described.

The optical technique chosen is the method of caustics by reflection, which has already found many useful applications in elastic dynamic fracture mechanics. This paper describes experiments designed to develop an extension of the method of caustics to applications in elastic-plastic fracture mechanics. The application of the present results to the analysis of dynamic experiments will be described in a future paper (Zehnder, Rosakis and Krisnaswamy, 1989).

The method of caustics was originally developed by Manogg (1964) for measuring the stress intensity factor in thin transparent, elastic plates. A series of important contributions on the subject is also summarized by Theocaris (1981). The first extensions of the method of caustics to elastic-plastic fracture were made by Rosakis and Freund (1982) and by Rosakis, Ma, and Freund (1983), based on the assumption of validity of the plane stress, HRR, asymptotic crack tip field (Hutchinson, 1968 and Rice and Rosengren, 1968) and it demonstrated that under certain conditions the value of the J integral *can* be measured with caustics. Nonetheless, the recent work of Zehnder, Rosakis and Narasimhan (1986) showed that the two-dimensional asymptotic approach severely limits the applicability of the method. This is true because such an analysis cannot deal with either three-dimensional effects near the crack tip or with large scale yielding effects, both characteristic of finite test specimens.

A new approach is taken here that allows for accurate measurement of thickness average of J for any planar test specimen geometry and material (Zehnder, 1987). In brief, the approach is to make a calibration of J versus the caustic diameter for a particular specimen geometry and material. It is shown that this calibration may be performed experimentally or numerically with equal accuracy. The results of simultaneous experiments, that use interferometry to measure the out of plane surface displacements of the specimen, give further insight into the limitations of previous attempts to analyze caustics through plane stress assumptions. The interferometric measurements are also used to confirm the accuracy of the three-dimensional finite element analysis described in Part I of this investigation and to discuss the region of dominance of the plane stress HRR field.

In the next section, the optical method of caustics is described and briefly reviewed. Subsequent sections describe experiments using the optical methods of caustics and Twymann-Green interferometry, performed simultaneously on either side of the test specimen. Load vs. load-point displacement and J vs. load records are also obtained experimentally. These records, as well as the out of plane surface

displacements, measured by interferometry, are compared with their numerical counterparts obtained on the basis of the 3-D calculation described in Part I. Finally the caustics experiments are used to obtain the relation between the caustic diameter, D, and the value of the J integral for different load levels. This is found to be in excellent agreement with the equivalent relation between D and J obtained numerically by means of the 3-D numerical calculation of Part I.

2. CAUSTICS BY REFLECTION

2.1 The mapping equations

Consider the flat surface of an opaque plate specimen of uniform thickness h, containing a through crack. In the undeformed state, this surface, assumed to be perfectly reflective, will occupy a region in the x_1, x_2 plane at $x_3 = 0$. When loads are applied on the lateral boundaries of the plate, the resulting change in thickness of the plate specimen is nonuniform and the equation of the deformed specimen surface will be expressed as:

$$x_3 + f(x_1, x_2) = 0 . \tag{2.1}$$

Consider further, a family of light rays parallel to the x_3-axis, incident on the reflecting surface. Upon reflection, the light rays will deviate from parallelism (see Figure 1). If certain geometrical conditions are met by the reflecting surface, then the virtual extensions of the reflected rays (dashed lines) will form an envelope which is a three-dimensional surface in space. This surface, called the *"caustic surface"*, is the locus of points of highest density of rays (maximum luminosity) in the virtual image space. The virtual extensions of the rays are tangent to the caustic surface. The reflected light field is recorded on a camera positioned in front of the specimen. The focal plane of this camera, which will be called the *"screen"*, is located behind the plane $x_3 = 0$ (occupied by the reflector in the undeformed state) and intersects the caustic surface at the plane $x_3 = -z_0$, $z_0 \geq 0$. On the *"screen"*, a cross section of the caustic surface is observed as a bright curve (the *caustic curve*), bordering a dark region (the *shadow spot*). The resulting optical pattern depends on the nature of the function $f(x_1, x_2)$ and on the focal distance z_0.

The reflection process can be viewed as a mapping of points (x_1, x_2) of the plane occupied by the reflector in the undeformed state, onto points (X_1, X_2) of the plane $x_3 = -z_0$ (the *"screen"*). The mapping equations based on geometrical optics are given by (Rosakis and Zehnder, 1985)

$$\underset{\sim}{X} = \underset{\sim}{x} - 2(z_0 - f)\,\frac{\nabla f}{1 - |\nabla f|^2} \tag{2.2}$$

where $\underset{\sim}{X} = X_\alpha \underset{\sim}{e}_\alpha$, $\underset{\sim}{x} = x_\alpha \underset{\sim}{e}_\alpha$, and $\underset{\sim}{e}_\alpha$ denote unit vectors. In the subsequent discussion Greek subscripts have the range 1,2.

When $z_0 \gg f$, as is usually the case in most practical applications, the above simplifies to

$$\underset{\sim}{X} = \underset{\sim}{x} - 2z_0 \nabla f \ . \tag{2.3}$$

Relations (2.3) are the mapping equations what will be used in the rest of this discussion.

2.2 The initial curve and its significance

Equation (2.2), or its approximation (2.3), is a mapping of the points on the reflecting surface onto points on the *"screen"*. If the *"screen"* intersects the caustic surface, then the resulting caustic curve on the *"screen"* is a locus of points for which the determinant of the Jacobian matrix of the mapping equations (2.3) must vanish or

$$I(x_1, x_2, z_0) = \det[X_{\alpha,\beta}] = \det[\delta_{\alpha,\beta} - 2z_0 f_{\alpha,\beta}] = 0 \ . \tag{2.4}$$

The above is a necessary and sufficient condition for the existence of a caustic curve. The locus of points on the reference plane (x_1, x_2, $x_3 = 0$) for which the Jacobian vanishes is called the *initial curve* and its equation is given by (2.4). All points on the initial curve map onto the caustic curve. In addition, all points inside and outside this curve map *outside* the caustic. Since the light that forms the caustic curve originates from the *initial curve*, essential information conveyed by the caustic comes from that curve *only*.

Equation (2.4), defining the initial curve, depends parametrically on z_0. Thus by varying z_0, the initial curve position may be varied. If z_0 is large, then the initial curve will be located far from the crack tip. If z_0 is small, then the initial curve will be close to the crack tip. Variation of z_0 can easily be achieved experimentally by simply varying the focal plane of the recording camera system. This is an essential property of the method of caustics and it can be utilized to "scan" the near tip region to obtain information regarding the nature of deformation field at different distances from the crack tip. For the case of a crack tip surrounded by a plastic zone, varying z_0 will move the *"initial curve"* inside or

outside the plastic zone, providing information on the plastic strains as well as on the surrounding elastic field.

2.3 The interpretation of caustics on the basis of plane stress analyses

The discussion of the previous section is intentionally kept as general as possible, and is not restricted by the form of the function $f(x_1, x_2)$ that describes the shape of the deformed specimewn surface. In general, $f(x_1, x_2)$ can be identified as the out of plane displacement field $u_3(x_1, x_2)$ evaluated on the surface of the plate specimen.

For a cracked plate of uniform thickness and finite, in-plane dimensions, u_3 will depend on the constitutive law of the material, on the applied load, and on the details of the specimen geometry (in-plane dimensions and thickness). Given the lack of full-field, three-dimensional analytical solutions in fracture mechanics, such information must be obtained by numerical computation. Nevertheless, there exist certain special cases where available asymptotic solutions, based on two-dimensional analyses, may provide adequate approximations for the surface out of plane displacement field $u_3(x_1, x_2)$. In particular, it can be argued that conditions of plane stress will dominate in thin, cracked plates provided that both the crack length and the in-plane dimensions are many times the plate thickness. In such cases, $u_3(x_1, x_2)$ can be approximated by means of available analytical solutions based on plane stress analyses.

2.3.1 Caustics obtained on the basis of plane stress aymptotic crack tip fields in linear elastostatics.

In linear elastic fracture mechanics, the principal application of the method of caustics is to the direct measurement of the mode-I and mode-II stress intensity factors. By substitution of the u_3 displacements for a Mode-I, plane stress crack (Williams, 1957) into equations (2.3) and (2.4), it was shown by Manogg (1964) (see also Theocaris (1981) and Beinert and Kalthoff (1981)) that K_I is related to the maximum transverse diameter D of the caustic (width of caustic in the direction perpendicular to the crack line) by

$$K_I = \frac{ED^{5/2}}{10.7 z_0 \nu h}, \tag{2.5}$$

where E is the elastic modulus, ν is the Poisson's ratio, h is the specimen thickness, and K_I is the mode-I stress intensity factor.

The equation for the initial curve is obtained directly from (2.4) and can be shown to be a circle of radius r_0 where

$$r_0 = 0.316 D = \left[\frac{3h \nu K_I z_0}{2E \sqrt{2\pi}} \right]^{2/5} \tag{2.6}$$

It should be observed here that for a given K_I, $r_0 \sim z_0^{2/5}$. A variation in z_0, the distance behind the specimen at which the camera is focussed, will result in changes in r_0.

2.3.2 Caustics obtained on the basis of the asymptotic, plane stress HRR field.

For stationary cracks and within the framework of small displacement gradients and proportional stress histories the value of the J-integral can be considered as a plastic strain intensity factor. The viewpoint is adopted here that J is the scalar amplitude of the deformed shape of the surface of an elastic-plastic fracture specimen at points within the region of dominance of the *plane stress* HRR field.

Substitution of the u_3 displacement given by the plane stress HRR fields into equations (2.3) and (2.4) provides a relation between D and J, found by Rosakis, Ma, and Freund (1983) to be

$$J = S_n \frac{\sigma_0^2}{E} \left[\frac{E}{\sigma_0 z_0 h} \right]^{\frac{n+1}{n}} D^{\frac{3n+2}{n}}, \tag{2.7}$$

where σ_0 is the yield stress, n is the hardening exponent for the Ramberg-Osgood material model and S_n is a scalar function of n tabulated by Rosakis, Ma, and Freund (1983). Unlike the elastic case, the initial curve is no longer circular; its shape depends on the hardening level of the material. It should be noted at this point that equations (2.5)-(2.7) are obtained under the assumption of the validity of particular asymptotic plane stress fields.

2.4 Limitations of 2-D asymptotic analyses

The results of previous experiments and analyses by Zehnder, Rosakis, and Narasimhan (1986) show that the interpretation of caustics on the basis of plane stress, small scale yielding assumptions limits the applicability of the technique for practical applications in elastic-plastic fracture mechanics to small scale yielding conditions in thin plates. Several factors combine to cause these limitations. Under small scale yielding conditions, the region of dominance of the plane stress HRR fields is $r < .3r_p$ where r_p is the plastic zone size ahead of the crack tip. Thus, to use equation (2.7) to measure J, the initial curve must satisfy $r_0 < .3r_p$. However, near the crack tip ($r < .5h$) there is a region where the deformation field is three-dimensional. Thus, unless $r_0 > .5h$, it is clear that interpretation of caustics obtained from near the crack tip and analyzed on the basis of the plane stress HRR field will be inaccurate. In most test specimens, it is not possible to satisfy the conflicting requirements $r_0 < .3r_p$ and $r_0 > .5h$.

In the next section, an approach is described which will allow for the measurement of the J integral with caustics regardless of specimen dimensions and load level. In brief this approach is a calibration of J versus the caustic diameter, D, for a particular three-dimensional specimen configuration. This calibration is performed both experimentally and numerically by means of a three-dimensional elasto-plastic calculation (see Part I). The two calibrations are compared to establish agreement between the experiment and the numerical calculation. As one might think, a specimen dependent calibration of this sort is not of particular use for static measurements of J where other techniques, based on boundary value measurements, can be used. On the other hand, such a calibration, will allow, for the first time, the interpretation of caustics obtained from a dynamic experiment by means of high-speed photography.

3. DESCRIPTION OF EXPERIMENTS

The investigation described in the following sections is both experimental and numerical. Caustic curves were obtained from a particular specimen configuration at different load levels and were compared to synthetic caustics obtained by finite elements and corresponding to the same load levels. The elastic-plastic finite element analysis of Part I modelled the exact three-dimensional specimen configuration and material constitutive properties. In order to provide an additional direct comparison between the computation and the actual specimen deformation, a second experiment was performed simultaneously with the caustics experiment. By using Twyman-Green interferometry, the out of plane displacement on the specimen surface was measured for load levels up to fracture initiation. These

displacements were compared direcctly to the numerical results. In addition the load and load point displacement were compared to the numerical results. These experiments used three point bend specimens (numbers 67 and 69) with a 4:1 length to width ratio. The specimen dimensions are given in Figure 2. The material used was 4340 steel, heat treated at 843° C for 1.5 hours, oil quenched, then annealed for 1 hour at 538° C. The material properties were yield stress $\sigma_0 = 1030$ MPa, and hardening exponent $n = 22.5$ for a fit to the piecewise power hardening law. In uniaxial tension this is equivalent to

$$\frac{\varepsilon}{\varepsilon_0} = \begin{cases} \sigma/\sigma_0 & \sigma \le \sigma_0 \\ (\sigma/\sigma_0)^n & \sigma > \sigma_0 \end{cases}, \tag{3.1}$$

where ε_0 is the yield strain. For these experiments both sides of the specimen were lapped optically flat and polished to a mirror finish to allow for simultaneous caustics and interferometry measurements.

Four measurements were performed on each specimen: caustics, interferometry, load, and load point displacement. The experiments proceeded by loading the specimen in small steps. During the loading the load cell and the load-point displacement signals were recorded. When loading was stopped at a particular step caustics photographs and interferometric photographs (interferograms) were recorded. This process was repeated until the point of fracture initiation.

3.1 Load and Load-Point Displacement

The load and load point displacement were recorded with a 100,000 lb. capacity load cell and a strain gage extensometer. The signals were recorded during loading by a digital oscilloscope. A photograph of the specimen and loading fixtures is shown in Figure 3. The extensometer was attached to fixtures connected to points "A" and "B" in the figure. There exists some extraneous displacement due to compliance of the loading fixtures, and indentation of the specimen at the contacts with the rollers. This extraneous displacement was subtracted using the procedure of Robinson and Tetelman (1967). In this procedure, the support rollers are placed together, and an uncracked specimen is inserted between the support rollers and the loading roller. The entire system is then compressed and the load-load point displacement is measured. It was found that the extraneous displacement was approximately linear with load and could be approximated by $\frac{\delta}{P} = 4.0 \times 10^{-6}$ mm/N, where δ is the load point displacement and P is the applied load.

3.2 Caustics

The caustics were photographed by means of the experimental arrangement shown in Figure 4. The collimated laser light reflected from the surface of the specimen is collected by the lens, which then forms an image of the caustic on the screen. The translucent screen (made of graph paper taped over plexiglass) is then photographed with the 35 mm camera. In these experiments z_0 was held constant. A preliminary experiment was performed to choose a suitable z_0. In the preliminary experiment, caustics were obtained for various z_0 values and load levels. At low loads the caustics were clear for all z_0's. But, as the load increased, as demonstrated in Figure 5, where a series of caustics for a fixed load corresponding to J = 190 kN/m and varying z_0's is shown, the caustics for small z_0's become blurred and ill-defined. This is caused partially by a loss of reflectivity due to plastic deformation. On this basis it was decided to use z_0 = 100 cm. This choice allows caustics to be recorded without loss of definition up to the fracture initiation load.

3.3 Inteferometry

A version of the Twyman-Green interferometer (see Hecht and Zajac, 1979) was used to measure the out-of-plane surface displacement, u_3. A sketch of the optical arrangement is shown in Figure 4. Due to the high sensitivity of interferometry, minimization of vibration of the specimen and optics is important. Thus the entire apparatus including the loading frame was mounted on an isolated optical table. The loading frame, optical table, camera, beam splitter and mirror are all seen in the photograph of Figure 3.

A 50 mm diameter, collimated laser beam, split into two with a beamsplitter, was used for the interferometer. As sketched in Figure 4, the reference beam reflects from the flat mirror back through the beamsplitter and into the camera. The object beam reflects from the specimen and then reflects from the beamsplitter into the camera. When the two beams are adjusted to fall on top of each other, any nonuniform differences in optical path length between the two beams results in light and dark fringes. For complete interference between the reference and object beams the intensity of light from each beam must be matched. Polished steel has a reflectivity of 50%, thus to match the reference beam to the object beam and 50% reflectance mirror was used. The fringe patterns were photographed with a 35 mm camera using a 200 mm f/4 (50 mm diameter) telephoto lens. The camera was located such that 50 mm of the specimen filled 25 mm on the film. Kodak Technical Pan 2415 film shot at ASA 100 and developed in Kodak D-19 was used in order to achieve high contrast and high resolution.

Destructive interference between two waves occurs when the waves are out of phase by $n\lambda/2$ where λ is the wavelength and $n = 1,3,5 \cdots$. The phase shift between the reference and object beams is equal to the difference in optical path length, thus the change in optical path length, δS, represented by adjacent dark fringes is $\delta S = \lambda$. For small deformations $S = 2u_3$, thus adjacent dark fringes represent a change in u_3 of $\delta u_3 = \lambda/2$. For the He-Ne laser used here $\lambda = .632\mu m$.

Due to the angular deflection of the reflected light rays, as seen in Figure 1, the relation $S = 2u_3$ is not completely accurate; the actual optical path is slightly larger. In addition, the angular deflection will change the location of the fringes. It was demonstrated by Zehnder (1987) that for these experiments the maximum error in fringe location is less than 1λ and the error is less than $.01\lambda$ in the u_3 values. It is important to focus the camera on the surface of the specimen so that a large caustic will not be formed, obscuring the crack tip. By minimizing the caustic, fringes can be resolved to within approximately 2 - 3 crack opening displacements.

The interferograms were analyzed by making 50X enlargements and digitizing the fringes by eye on a computer digitizing pad.

4. NUMERICAL CALCULATIONS

The numerical calculations of Part I of this investigation, (Narasimhan and Rosakis, 1988b) modelled in three dimensions, one quarter of the three point specimen shown in Figure 3, using five layers of elements for half the thickness. An incremental J_2 plasticity theory was used. The material obeyed the von Mises yield criterion and followed the piecewise power hardening law of equation (3.1), with $n = 22.5$ and $\sigma_0 = 1030$ MPa, corresponding to the material used in the experiment. Loads were applied to the specimen incrementally going from 0 to 80,000 N. The J integral calculated in Part I of this investigation is shown here as a function of load in Figure 6. This J corresponds to an integral evaluated over a cylindrical surface surrounding the crack front and can be shown to be equal to the thickness average of the local definition of J along the crack front.

5. RESULTS: COMPARISON BETWEEN EXPERIMENTS AND CALCULATIONS

5.1 Load, Load-Point Displacement and J Integral

The specimen geometry was chosen to take advantage of the load-displacement methods for estimating the J integral. For a ductile three-point bend specimen, Rice, Paris, and Merkle (1973) showed that J may be estimated by

$$J = \frac{2}{hC} \int_0^{\delta_c} P d\delta_c \ , \tag{5.1}$$

where P is the load applied to the specimen, h is the specimen thickness, and C is the uncracked ligament length. The quantity δ_c is the load point displacement due to the presence of the crack, i.e., $\delta_c = \delta - \delta_{nc}$ whre δ is the total load point displacement and δ_{nc} is the load point displacement of an uncracked, elastic beam of the same dimensions as the fracture specimen.

The load-displacement ($P - \delta$) curves for specimens 67 and 69 are shown in Figure 7. For each specimen, points are plotted only up to fracture initiation (74,700 N or $.98P_0$ where P_0 is the plane stress limit load). Also shown is the $P - \delta$ curve calculated from the three-dimensional numerical model (see Part I of this investigation). Comparison of these results shows very good agreement between the experiments and the calculations.

The resulting J integral, plotted as a function of load, P, is given in Figure 6. Shown in the figure are J calculated from equation (5.1) using the experimental results and J calculated from the numerical analysis (see Part I). The agreement between the numerical and experimental results is quite good, indicating that J may be calculated accurately either way. In the following discussions, the relation between J and the applied load P shown in Figure 5 is used.

5.2 Interferometry and u_3 Comparison

Since it is displacements that are most accurately calculated in the finite element method, these are chosen for the most direct comparison with experiments. Interferograms were recorded for load levels from 6000 N up to fracture initiation (74,700 N). At the highest load levels the quality of the interferograms deteriorates. This is due to the roughening of the surface, resulting from plastic deformation near the crack tip and also due to the high fringe density near the crack tip. The highest load for which

fringes very near the crack tip could be resolved was 57,300 N.

Typical interferograms are presented in Figures 8 and 9. Figure 8 provides an overall picture of the out-of-plane displacement field for a region of approximately 4 cm diameter. A more detailed view of the near tip region is shown in Figure 9. Figure 9 shows that fringes can be resolved almost all the way up to the crack tip (up to three crack opening displacements) except for the part obscured by a small caustic.

Each interference fringe represents a line of constant out of plane displacement on the specimen surface. Thus the interferogram is a contour map of the specimen surface. The numerical contour map on the bottom of Figure 9 is a synthetic interferogram obtained from the out of plane displacements calculated from the three-dimensional numerical model in Part I. The displacement increment between the lines is the same as in the optical interferogram (.317 μm). As is evident from this comparison, good qualitative agreement of the experimental and synthetic interferograms is achieved.

The interferograms represent the u_3 displacement of the specimen with respect to some plane, the plane of the reference mirror. The mirror is aligned as close to parallel to the specimen as possible. Nonetheless, it will usually deviate slightly from parallelity. This deviation can be accounted for if the displacements are known at 3 or more noncollinear points on the specimen. The u_3 results from the interferograms are matched to known displacements at these points. Due to the Mode-I symmetry of the specimen and loading used in this experiment, the number of required points is reduced to two points not on a line parallel to the x_2 axis. The know displacements at the two points were provided by the finite element calculation. The points used ($x_1 = -1.5cm, x_2 = 0$ and $x_1 = 2.1cm, x_2 = 0$) are points of zero u_3 displacement.

The u_3 displacement along the line $\theta = 0$ is shown in Figure 10 for three load levels. Data are shown only as close to the crack tip as fringes could be resolved. Generally fringes could be measured to approximately 0.3 mm ahead of the crack tip and to approximately 0.5 mm behind the crack tip. Away from the crack tip u_3 is linear with x_1 as it should be for a beam. The displacement crosses zero at $x_1 = 2.1$ cm and is positive for greater x_1 values since this part of the specimen is in compression. The displacement gradients are much larger behind the crack tip than ahead of the crack tip. The plastic zone does not spread much behind the crack tip. Since most of the displacement occurs within the plastic zone, this displacement must occur over a small distance, causing the steep displacement gradients.

To help visualize what the u_3 field looks like near the crack tip, the experimentally obtained u_3 is plotted three dimensionally in Figures 11a and 11b for two different views. These compare well with the equivalent surface plots shown in Figure of Part I.

A quantitative comparison between the experimental and numerical results is given in Figures 12-14. In these figures, the experimentally obtained out of plane displacement, u_3, along the line $x_2 = 0$ is plotted as a function of normalized distance x_1 from the crack tip for three load levels. Also shown are the numerical results for the displacements corresponding to the same load levels. For reference, the extent of the plastic zone ahead of the crack tip as well as the distance corresponding to one half the specimen thickness are also shown on the figures. In Figure 12, where the plastic zone is very small, u_3 from the linear elastic plane-stress K_I field is shown for comparison. In Figure 14, where the plastic zone is larger, u_3 from the plane stress HRR field is given.

The first observation is the excellent agreement between the experimental and numerical results at all load levels. To show that the angular variation in displacement of the numerical results is also accurate, the numerical and experimental u_3 along the line $\theta = 40°$ is given in Figure 15 for a load of 52,300 N. Again the agreement of numerical and experimental results is excellent.

For all load levels (see in particular Figure 14), it was found that there is no region where the plane stress HRR field adequately described u_3 on the specimen surface. The asymptotic HRR field does not agree with the actual field because of three dimensionality of the near crack tip fields and because of the limited range of dominance of the asymptotic solution. At low loads Figure 12 shows that the plane stress K_I field differs from the calculated u_3 by approximately 25% for reasons similar to the ones discussed above. However, the method of caustics as based on the K_I field could probably be used for these specimens at low loads since the experimentally obtained slope of u_3 is close to that predicted by the K_I field when $r_0 \simeq .5h$. Recall that caustics depend on ∇u_3, not on the absolute value of u_3.

Recent experiments by Chiang and Hareesh (1986) on very thin, ductile specimens showed that the HRR field does predict u_3 and u_2 accurately for $r/h > 1$. In those experiments the ratio of specimen width to thickness was 30:1. In the present experiments the ratio is 7:1. The results of Chiang and Hareesh indicate that if one can make measurements in a region far enough away from the crack tip so that three-dimensional effects are negligible, but close to the crack tip compared to in-plane specimen dimensions, then the asymptotic fields will accurately describe the true fields in some finite region. The location of such a region will depend on specimen geometry and, if the material is non-linear, on the

applied load level. One puzzling result of Chiang and Hareesh is that $-u_3$ has a maximum not at the crack tip but at $r/h \simeq 0.5$. This result is contradicted by both the present investigation and by results of Wu and Chiang (1986) that show that $-u_3$ has its maximum at the crack tip. Perhaps the difference has to do with the differences in specimen geometries between the different experiments.

5.3 Caustics

In the previous section we were able to demonstrate that in terms of out of plane displacements, the numerical results are in excellent agreement with experiment. This indicates that it should be possible to generate caustics numerically which agree well with the experimentally observed caustics and are useful for the measurement of the J integral. In this section this hypothesis is tested.

Caustics are first recorded experimentally for specimens 67 and 69 using a *fixed value* of $z_0 = 100$ cm. The sequence of caustic patterns for increasing loads up to fracture initiation, is shown in Figure 16. For the same value of z_0, and the same loads, caustics are also generated numerically from the results of the 3-D finite element analysis. This was achieved by smoothing the u_3 displacements at the specimen surface obtained by the numerical solution using a least squares numerical scheme as described by Narasimhan and Rosakis (1988a). These displacements are shown in Figure 12 of Part I. Caustic patterns were simulated by mapping rays point by point from this smoothed surface using Equation (2.3). The numerically simulated caustics are also shown in Figure 16. All of the caustic curves, both experimental and numerical are reproduced here in the same scale. The values of J shown in the figure are related to the applied load through the J–P record of Figure 6. Figure 16 shows that there is good agreement, in shapes and sizes, between the experimental and numerical caustics.

Both experimental and numerical results were used to obtain a relation between caustic diameter D and the J integral which is shown in Figure 17 in a nondimensional form. J was obtained from Figure 6 and D was measured directly from the experimentally and numerically generated caustics. Also shown in the figure are the J vs. D relations obtained on the basis of the plane stress elastic analysis, equation (2.5), and on the basis of the plane stress HRR field, equation (2.7). The solid line in Figure 16 is a fit through the experimental and numerical data points.

It is seen that the experimental and numerical results are in excellent agreement. This demonstrates that such an approach can provide an accurate analysis of caustics in the form of a calibration for measuring the J integral. The best fit curve shown in Figure 17 serves here as an empirical relationship

between the caustic diameter and the J integral when the relationship based on two-dimensional asymptotic analyses are invalid. This relationship is valid only for the specimen geometry and material tested here and only for $z_0 = 100$ cm.

6. DISCUSSION

The above shows that all aspects of the numerical and experimental results are in good agreement. The numerical and experimental $P - \delta$ and $J - P$ results of Figures 6 and 7 show that the numerical calculation accurately models the overall specimen behavior. Also, it is demonstrated that J calculated from the experimental $P - \delta$ results, using equation (5.1), is consistent with the numerical calculation of J. This demonstrates that equation (5.1) can be used accurately to calculate J without resorting to a complicated 3-D numerical calculation. The agreement of the calculated and measured u_3 displacements (Figures 12-15) leaves no question that the numerical calculations are accurate and sufficiently refined to model this specimen well, both in the overall behavior and in the details of the crack tip fields. This provides a great deal of confidence in the numerical results and allows for the construction of accurate synthetic caustics. In addition as evident from Figure 17, it is demonstrated that the calibration of J versus D may be performed either experimentally or numerically with equal accuracy. In most cases, it will be more economical to perform this calibration experimentally.

The method of caustics as described in this paper is thus proposed as a technique for dynamic measurements of the J integral. A procedure is proposed as follows: Given a material to test, select a planar test specimen geometry that is adaptable to dynamic loading. Small scale yielding conditions need not be maintained, and there is virtually no restriction on thickness of the specimen. Prepare the specimens by lapping and polishing one surface. Perform a static calibration of J versus D for different load levels and a fixed z_0. Use the same specimen geometry and material in a dynamic experiment and record the caustics (with same fixed z_0) up to crack initiation by means of a high speed camera. Then use the calibration between J and D, described above, to analyze the caustics to determine the time history of J under dynamic loading conditions. Preliminary results on the implementation of the above procedure for the dynamical measurement of J are reported by Zehnder (1987) and by Zehnder, Rosakis and Krisnaswamy (1989).

The advantage of this procedure comes from the use of a local, near tip measurement for estimating J. This is expected to capture the details of time variation of J near the crack tip, even for high loading rates and short times compared to stress wave transit times of the specimen. It should be noted that such an approach is expected to be most accurate in strain rate insensitive solids. Its accuracy when applied to highly rate sensitive materials needs further investigation.

7. ACKNOWLEDGEMENTS

Support of the ONR contract N00014-85-K-0596 is gratefully acknowledged. The second author, (A.J. Rosakis) also acknowledges the support of the NSF-PYI Grant MSM-8451204. The computations were performed using the Supercomputer facilities at the University of California at San Diego. The authors would also like to thank Mr. Richard Pfaff for assistance and advice on the interferometry part of these experiments.

REFERENCES

Beinert, J. and Kalthoff, J. F. 1981 "Experimental Determination of Dynamic Stress Intensity Factors by the Method of Shadow Patterns," in *Mechanics of Fracture*, Vol. VII, G. Sih (ed.), Sijthoff and Noordhoff, pp. 281-320.

Chiang, F. P. and Hareesh, T. V. 1986 "Three Dimensional Crack Tip Deformation: An Experimental Study and Comparison to HRR Field," College of Engineering and Applied Sciences, Technical Report No. 481, State University of New York at Stony Brook, to appear in the *International Journal of Fracture* (1988).

Costin, L. S., Duffy, J. and Freund, L. B. 1977 "Fracture Initiation Under Stress Wave Loading Conditions," in *Fast Fracture and Crack Arrest*, ASTM STP 627, American Society for Testing and Materials, pp. 301-318.

Hecht, E. and Zajac, A. 1979 *Optics*, Addison-Wesley Publishing Company, pp. 322-324.

Hutchinson, J. W. 1968 "Singular Behavior at the End of a Tensile Crack in a Hardening Material," *Journal of the Mechanics and Physics of Solids*, Vol. 16, pp. 13-31.

Manogg, P. 1964 "Anwendungen der Schattenoptik zur Untersuchung des Zerressvorgags von Platten," Ph.D. Thesis, Freiburg, West Germany.

Nakamura, T., Shih, C. F. and Freund, L. 1985 "Elastic-Plastic Analysis of a Dynamically Loaded Circumferentially Notched Round Bar," *Engineering Fracture Mechanics*, Vol. 22, pp. 437-452.

Narasimhan, R. and Rosakis, A. J. 1988a "A Finite Element Analysis of Small-Scale Yielding Near a Stationary Crack Under Plane Stress," *Journal of the Mechanics and Physics of Solids* Vol. 36, No. 1, pp. 77-117.

Narasimhan, R. and Rosakis, A. J. 1988b "Three Dimensional Effects Near a Crack Tip in a Ductile Three Point Bend Specimen Part I: Numerical Analysis," Caltech Report SM88-6, submitted to *Journal of Applied Mechanics*.

Rice, J. R. 1968 "A Path Independent Integral and the Approximate Analysis of Strain Concentration by Notches and Cracks," *Journal of Applied Mechanics*, Vol. 35, pp. 379-386.

Rice, J. R. and Rosengren, G. F. 1968 "Plane Strain Deformation Near a Crack Tip in a Power-Law Hardening Material," *Journal of the Mechanics and Physics of Solids*, Vol. 16, pp. 1-12.

Rice, J. R., Paris, P. C. and Merkle, J. G. 1973 "Some Further Results of the J-Integral Analysis and Estimates," in *Progress in Flow Growth and Fracture Toughness Testing*, ASTM STP 536, American Society for Testing and Materials. pp. 231-245.

Robinson, J. N. and Tetelman, A. S. 1967 "Comparison of Various Methods of Measuring K_{IC} on Small Precracked Bend Specimens that Fracture after General Yield," *Engineering Fracture Mechanics*, Vol. 8, pp. 301-313.

Rosakis, A. J. and Freund, L. B. 1982 "Optical Measurement of Plastic Strain Concentration at a

Crack Tip in a Ductile Steel Plate," *Journal of Engineering Materials and Technology*, Vol. 104, pp. 115-120.

Rosakis, A. J., Ma, C. C., and Freund, L. B. 1983 "Analysis of the Optical Shadow Spot Method for a Tensile Crack in a Power-Law Hardening Material," *Journal of Applied Mechanics*, Vol. 50, pp. 777-782.

Rosakis, A. J. and Zehnder, A. T. 1985 "On the Method of Caustics: An Exact Analysis Based on Geometrical Optics," *Journal of Elasticity*, Vol. 15, pp. 347-367.

Shih, C. F., Moran, B., and Nakamura, T. 1986 "Energy Release Rate Along a Three-Dimensional Crack Front in a Thermally Stressed Body," *International Journal of Fracture*, Vol. 30, pp. 79-102.

Theocaris, P. S. 1981 "Elastic Stress Intensity Factors Evaluated by Caustics," in *Mechanics of Fracture*, Vol. VII, G. Sih (ed.), Sijthoff and Noordhoff, pp. 189-252.

Williams, M. L. 1957 "On the Stress Distribution at the Base of a Stationary Crack," *Journal of Applied Mechanics*, Vol. 24, pp. 109-114.

Wu, X. P. and Chiang, F. P. 1986 "Three Dimensional Crack-Tip Deformation in a Plastically Deformed Three-Point Bend Specimen," College of Engineering and Applied Sciences Technical Report No. 475, State University of New York at Stony Brook.

Zehnder, A. T., Rosakis, A. J., and Narasimhan, R. 1986 "Measurement of the J Integral with Caustics: An Experimental and Numerical Investigation," GALCIT SM Report 86-8, California Institute of Technology, to appear in an ASTM STP 995.

Zehnder, A. T. 1987 "Dynamic Fracture Initiation and Propagation in Metals: Experimental Results and Techniques," Ph.D. Thesis, California Institute of Technology.

Zehnder, A. T., Rosakis, A. J. and Krishnaswamy, S. 1989 "Dynamic Measurement of the J-Integral in Ductile Metals: Comparison of Experimental and Numerical Techniques." To appear in the *International Journal of Fracture*, Special Issue on Nonlinear Fracture Mechanics, (*Proceedings of the IUTAM Symposium on Recent Advances on Nonlinear Fracture Mechanics*, California Institute of Technology, March 14-16, 1988), edited by W. G. Knauss and A. J. Rosakis.

FIGURES

Figure 1.: Formation of caustic due to reflection of light from the polished, deformed specimen surface near the crack tip.

Figure 2.: (a) Three point bend test specimen. All dimensions are in centimeters. (b) Finite element mesh. (c) Details of finite element mesh near the crack tip.

Figure 3.: Photograph of loading frame and fixtures, specimen and interferometer optics.

Figure 4.: Optical setup for combined caustics and interferometry experiment.

Figure 5.: Sequence of caustics for a fixed load, but varying z_0.

Figure 6.: J integral versus applied load.

Figure 7.: Load-point displacement versus applied load.

Figure 8.: Interferogram corresponding to a load of 35,000 N.

Figure 9.: Comparison of experimental and numerical interferograms. Experimental interferogram is a magnification of Figure 8.

Figure 10.: Experimentally measured out-of-plane surface displacement for three different loads.

Figure 11a.: Experimental u_3 displacement for 52,300 N.

Figure 11b.: Experimental u_3 displacement for 52,300 N, (alternate view).

Figure 12.: Nondimensional u_3 displacement on the line $\theta = 0$. Comparison of experimental and numerical results for 21,200 N. Also shown is plane stress K_I field.

Figure 13.: Nondimensional u_3 displacement on the line $\theta = 0$. Comparison of experimental and numerical results for 35,000 N. Also shown is plane stress K_I field.

Figure 14.: Nondimensional u_3 displacement on the line $\theta = 0$. Comparison of experimental and numerical results for 52,300 N. Also shown is plane stress K_I field and u_3 from plane stress HRR field.

Figure 15.: Nondimensional u_3 displacement on the line $\theta = 40°$. Comparison of experimental and numerical results for 52,300 N.

Figure 16.: Sequence of caustics for increasing loads, $z_0 = 100$ cm. Experimental results from specimen 67. Numerical results for 3-D numerical analysis.

Figure 17.: Relation between caustic diameter D and J integral. Experimental and 3-D numerical results are shown. Also shown are relations from 2-D asymptotic analyses.

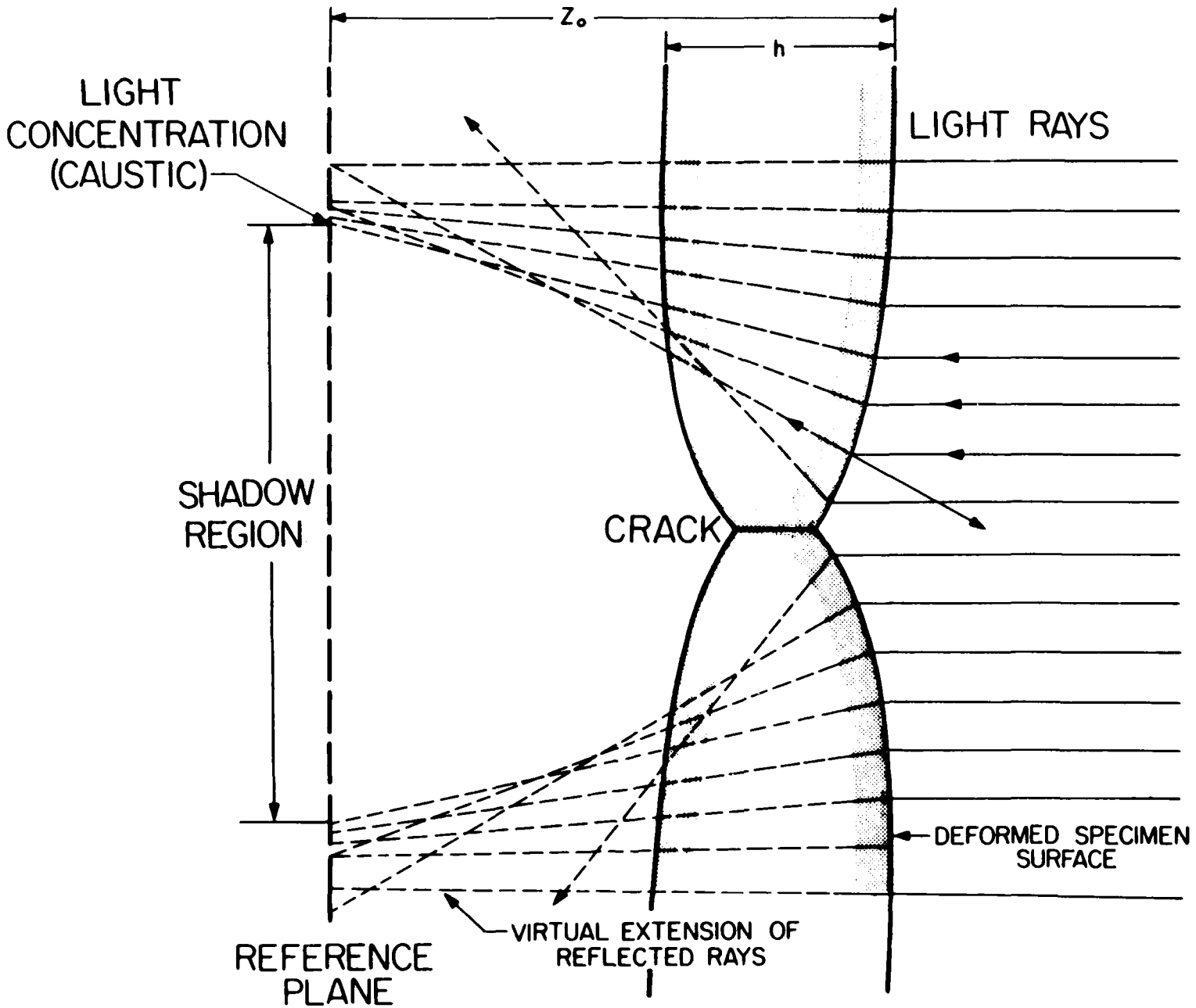

Figure 1.: Formation of caustic due to reflection of light from the polished, deformed speci-

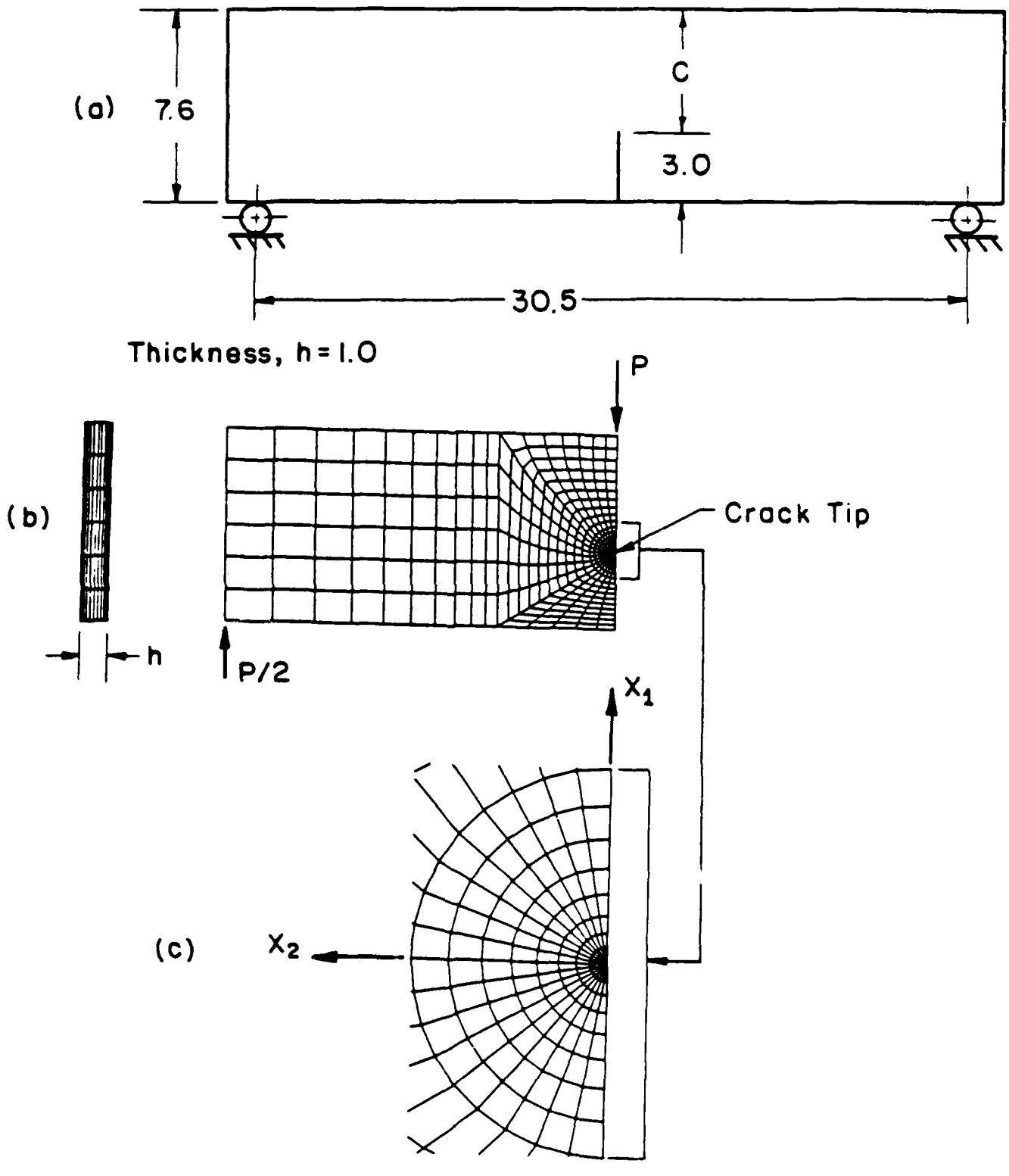

Figure 2.: (a) Three point bend test specimen. All dimensions are in centimeters. (b) Finite element mesh. (c) Details of finite element mesh near the crack tip.

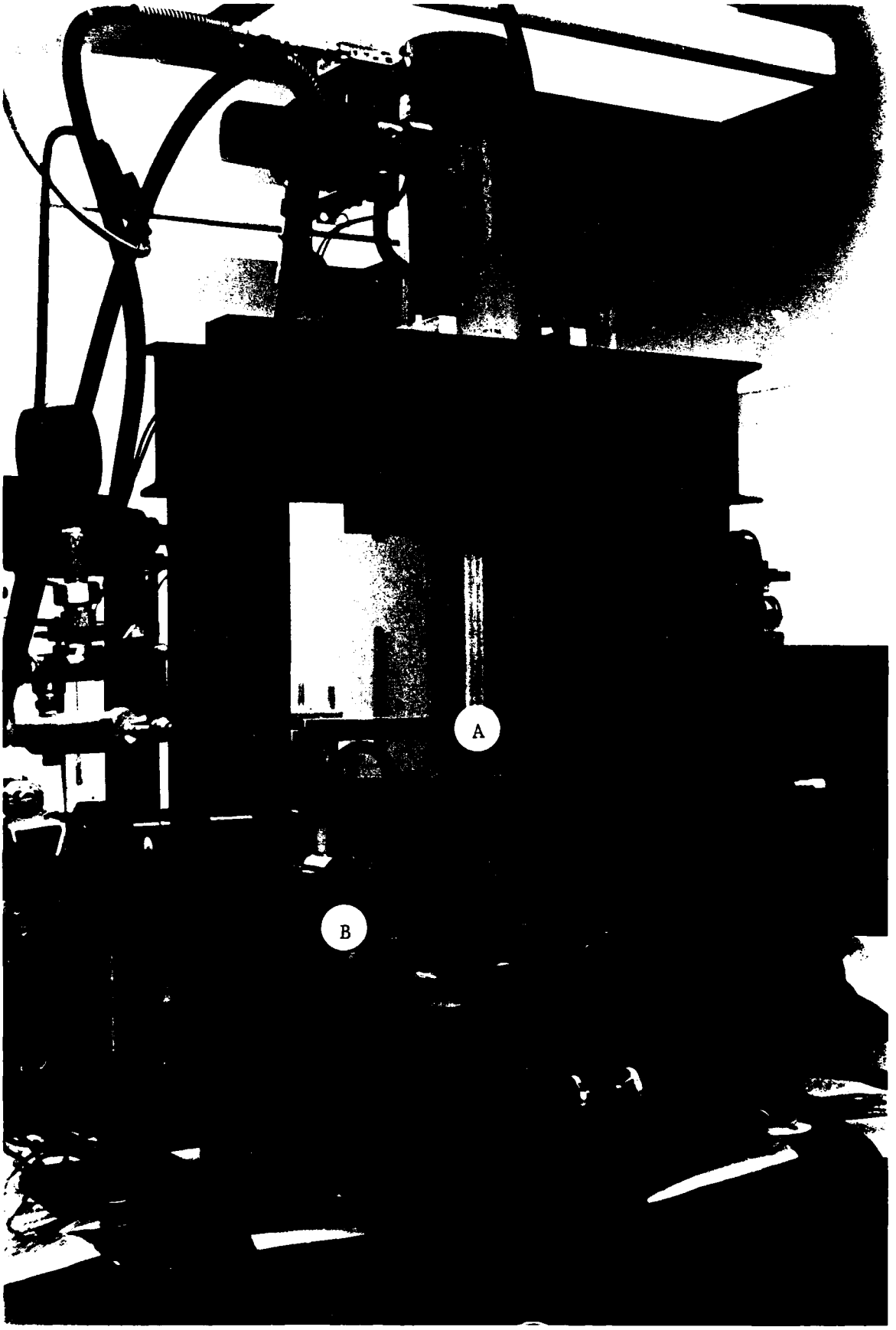

Figure 3.: Photograph of loading frame and fixtures, specimen and interferometer optics.

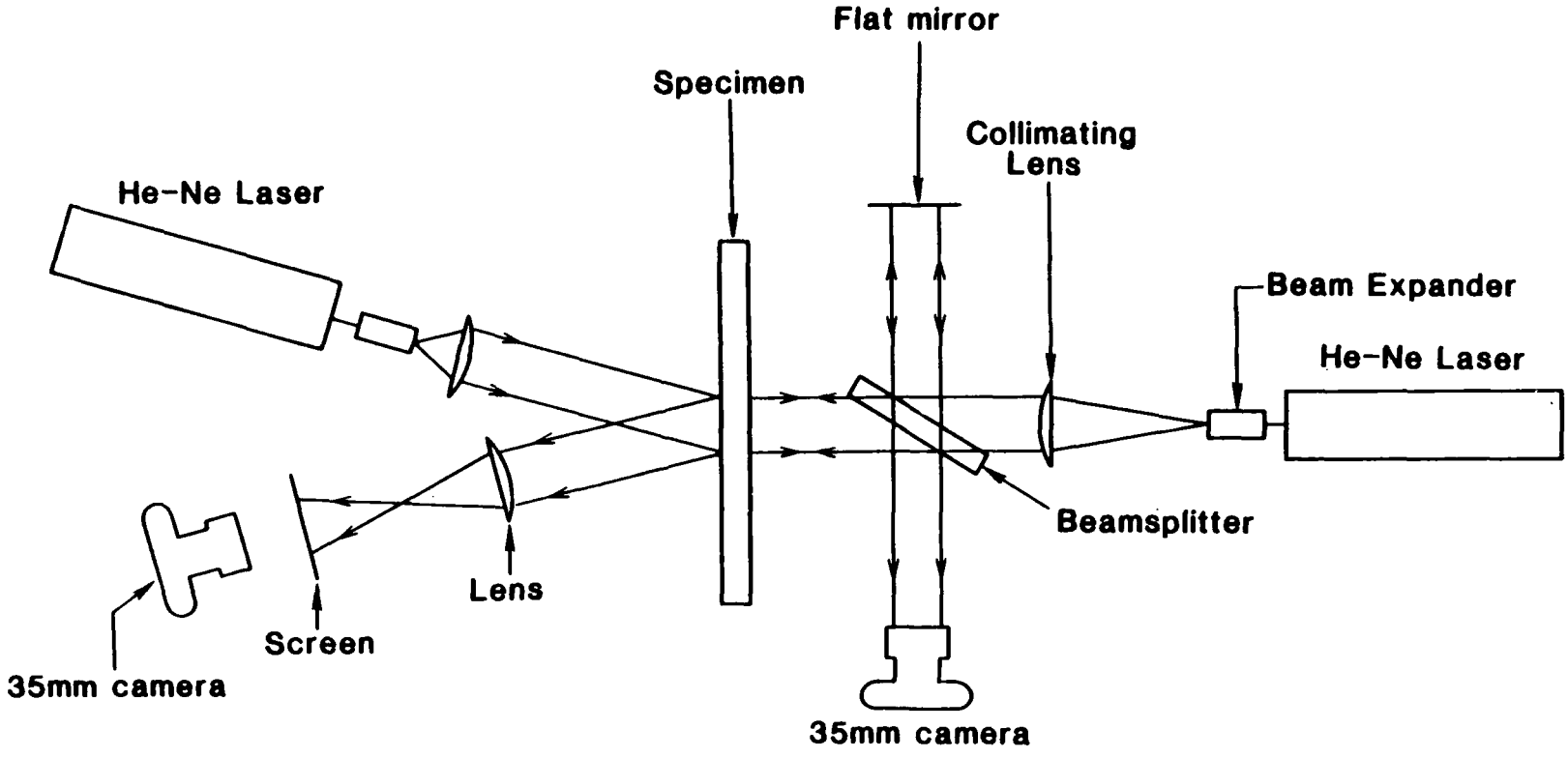

Figure 4.: Optical setup for combined caustics and interferometry experiment.

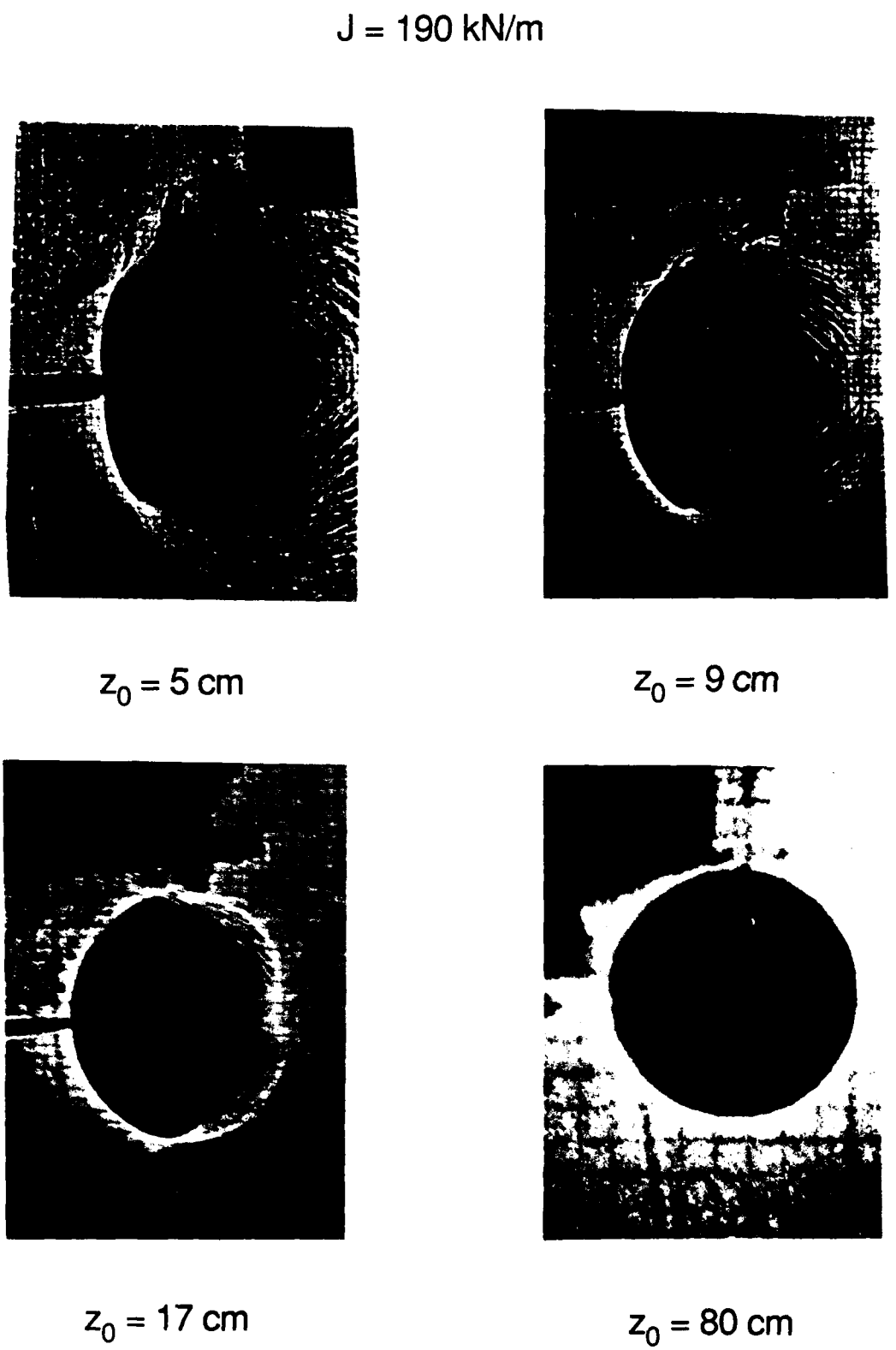

Figure 5.: Sequence of caustics for a fixed load, but varying z_0.

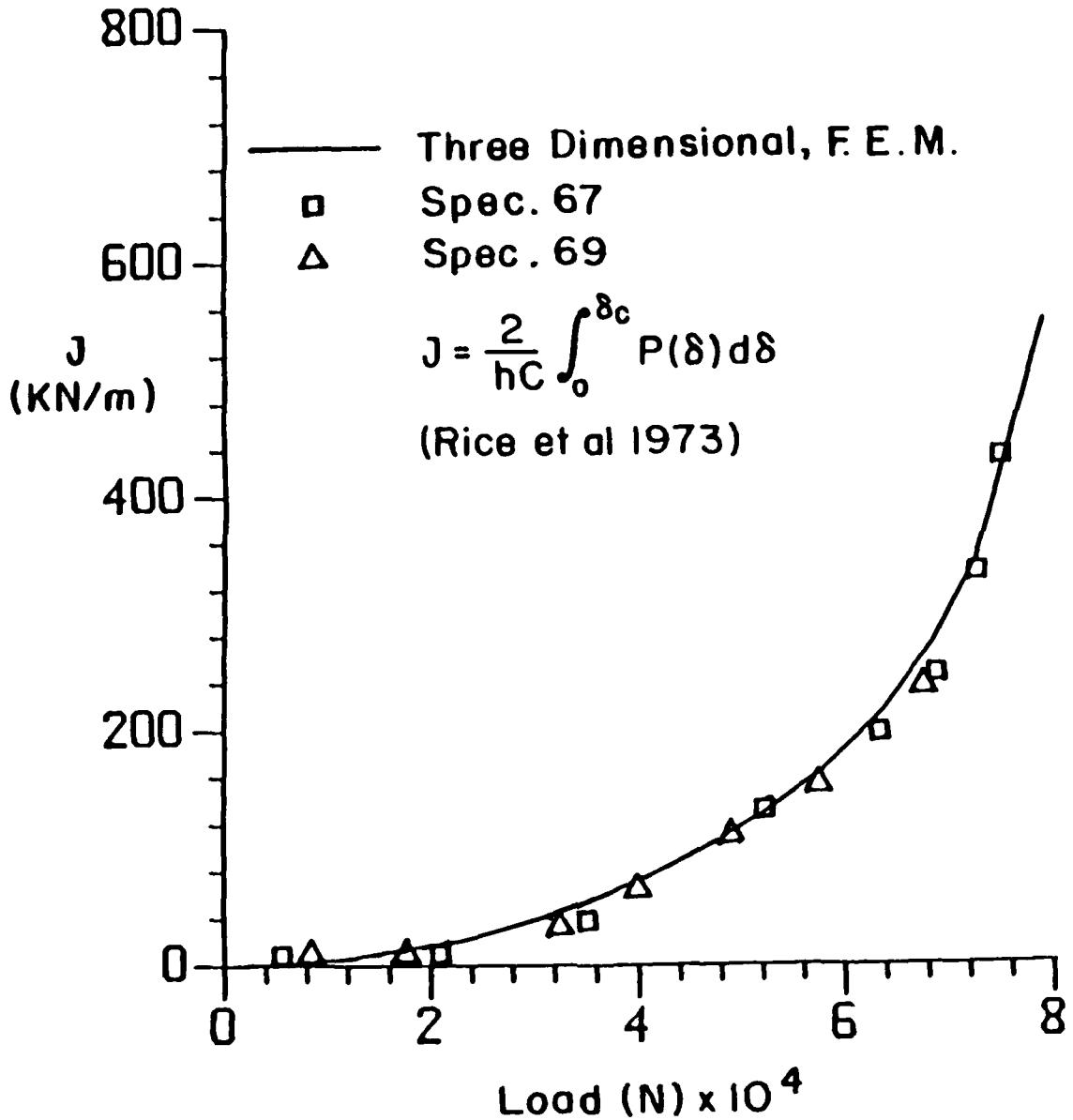

Figure 6.: *J* integral versus applied load.

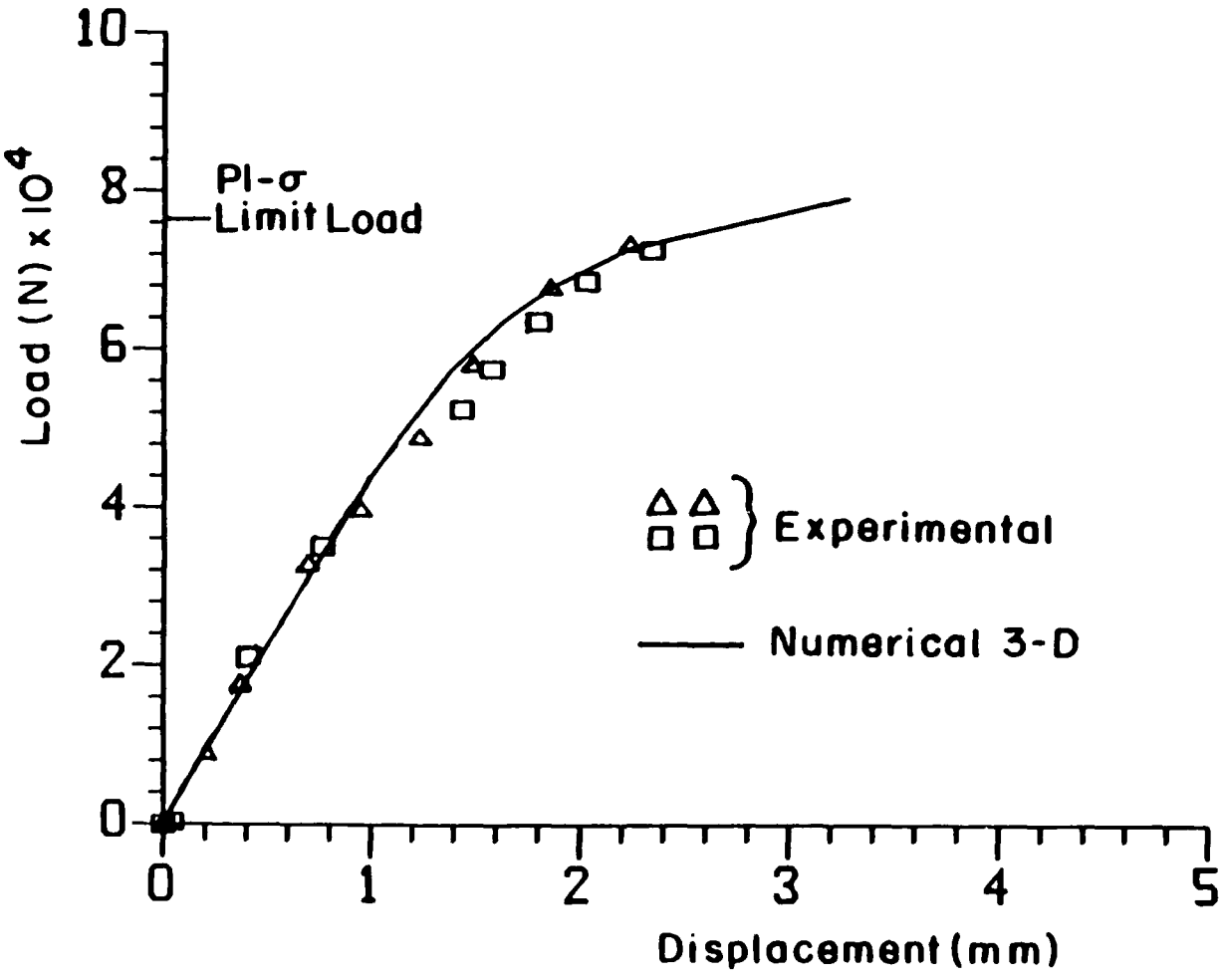

Figure 7.: Load-point displacement versus applied load.

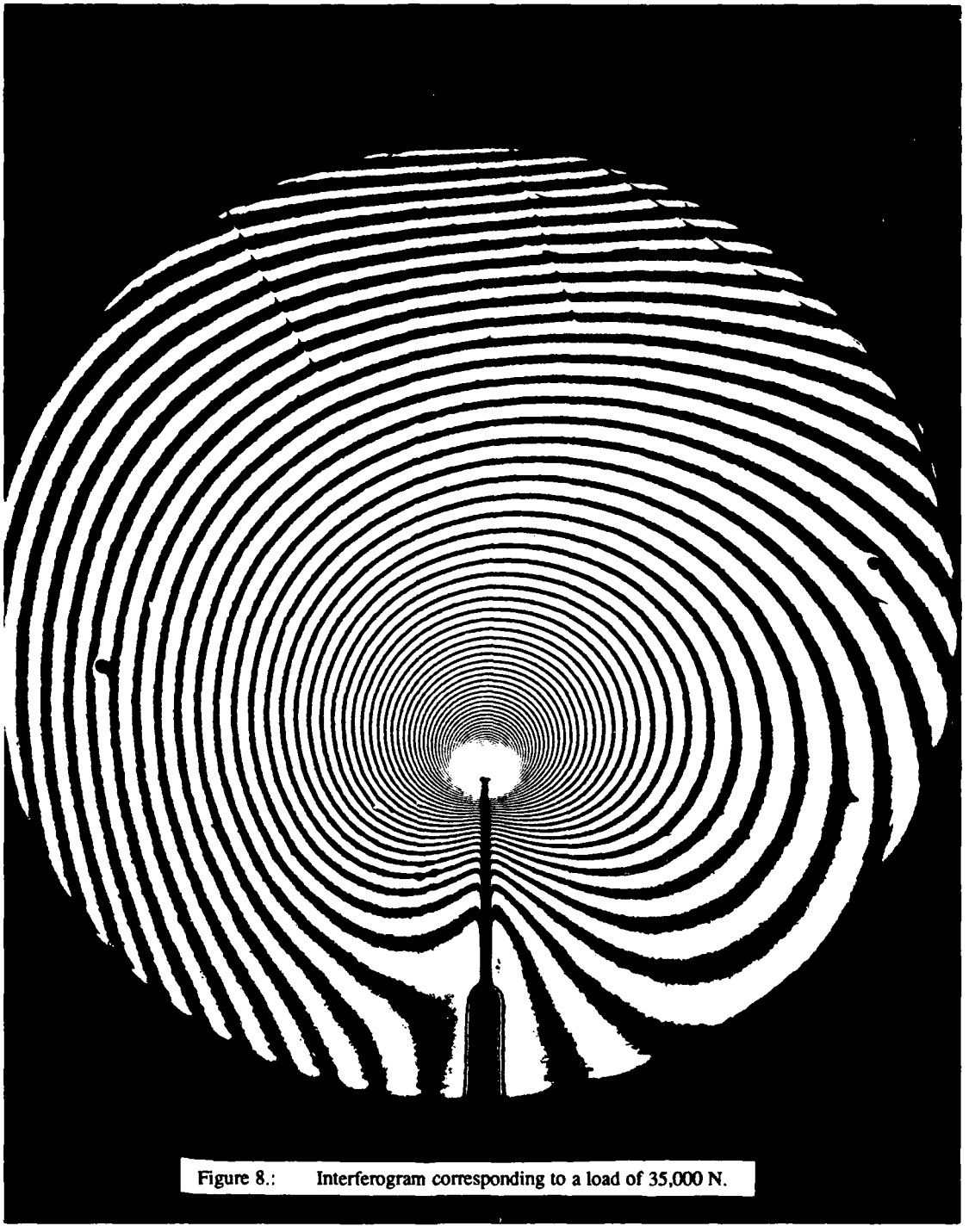

Figure 8.: Interferogram corresponding to a load of 35,000 N.

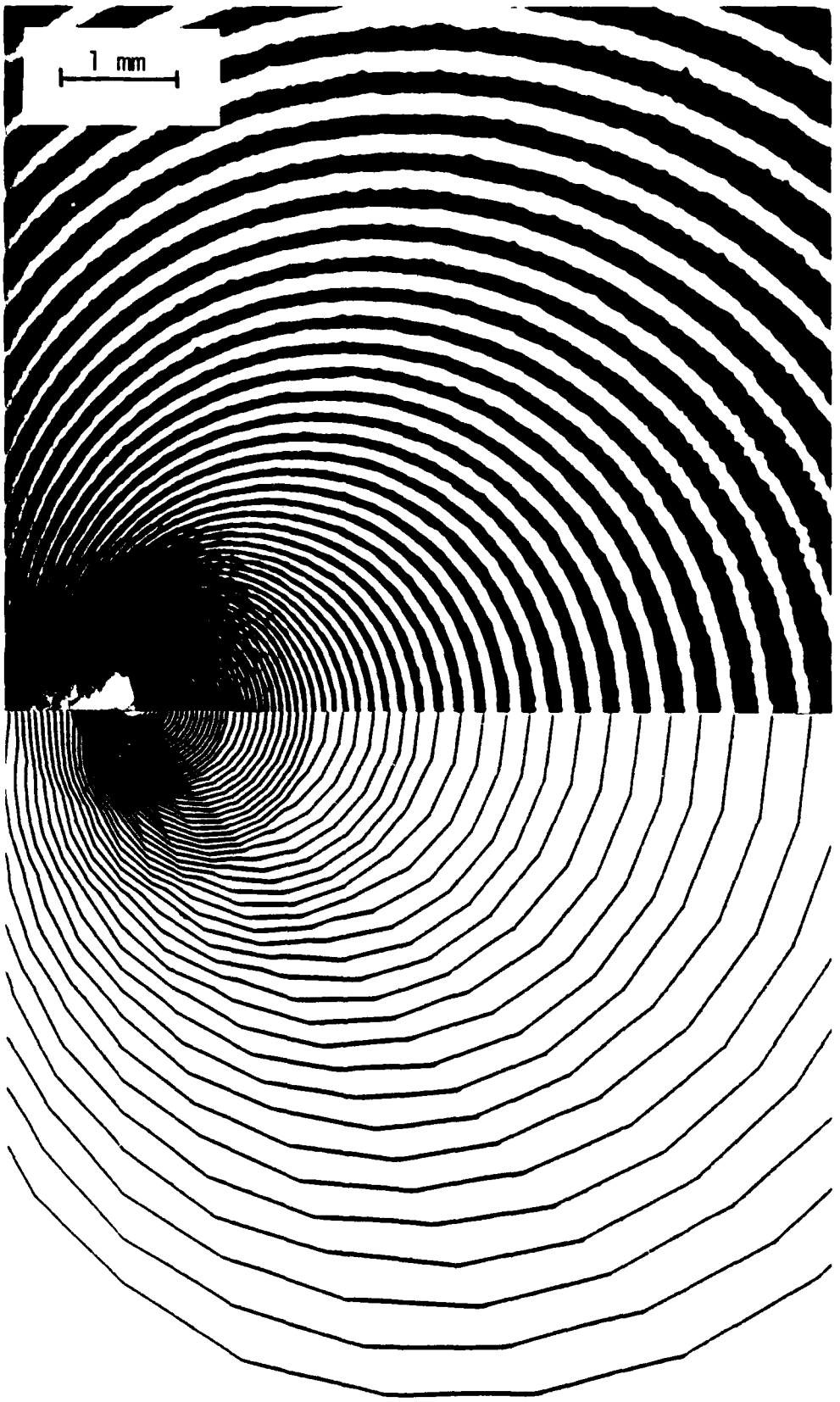

Figure 9.: Comparison of experimental and numerical interferograms. Experimental interferogram is a magnification of Figure 8.

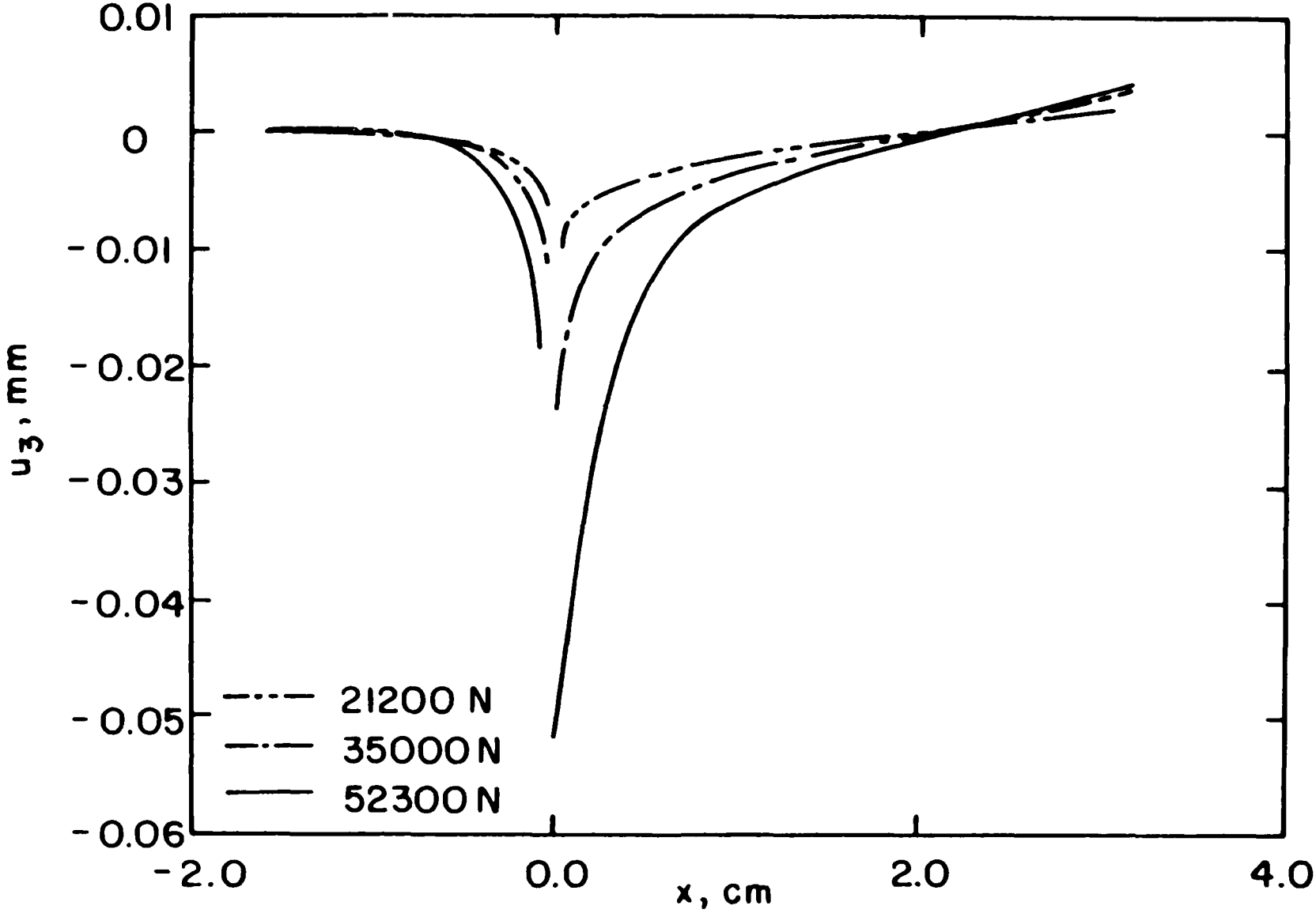

Figure 10.: Experimentally measured out-of-plane surface displacement for three different loads.

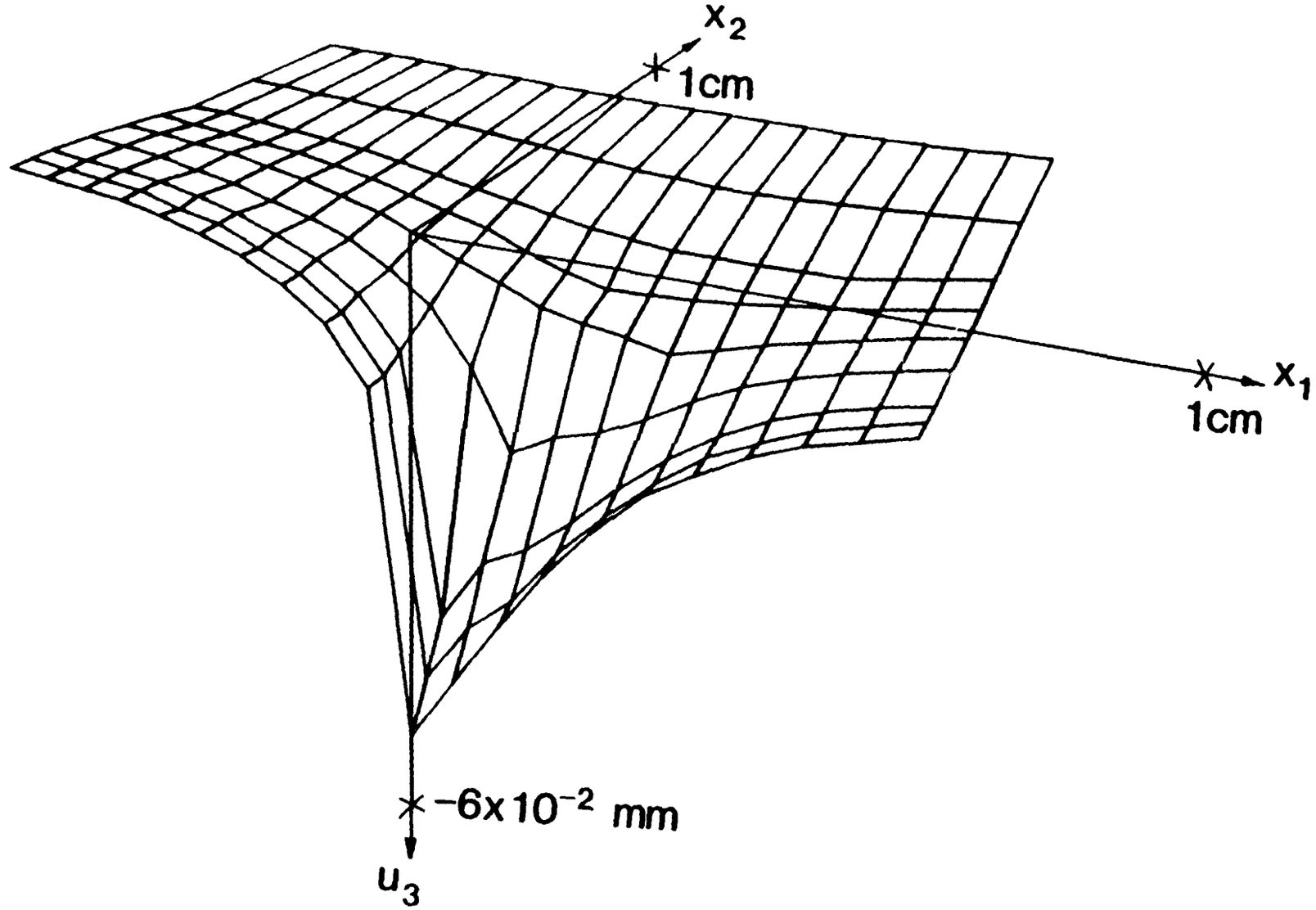

Figure 11a.: Experimental u_3 displacement for 52,300 N.

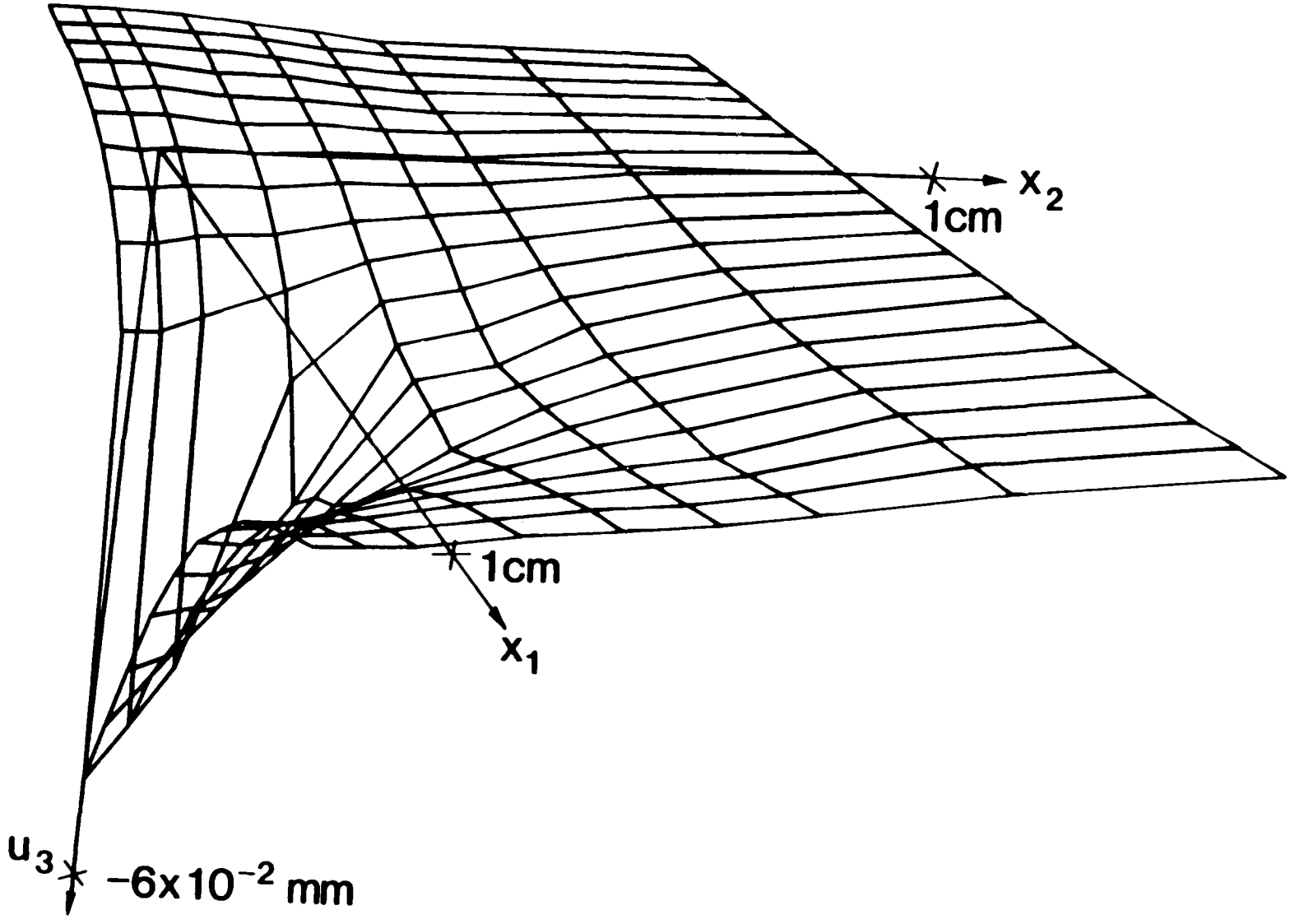

Figure 11b.: Experimental u_3 displacement for 52,300 N, (alternate view).

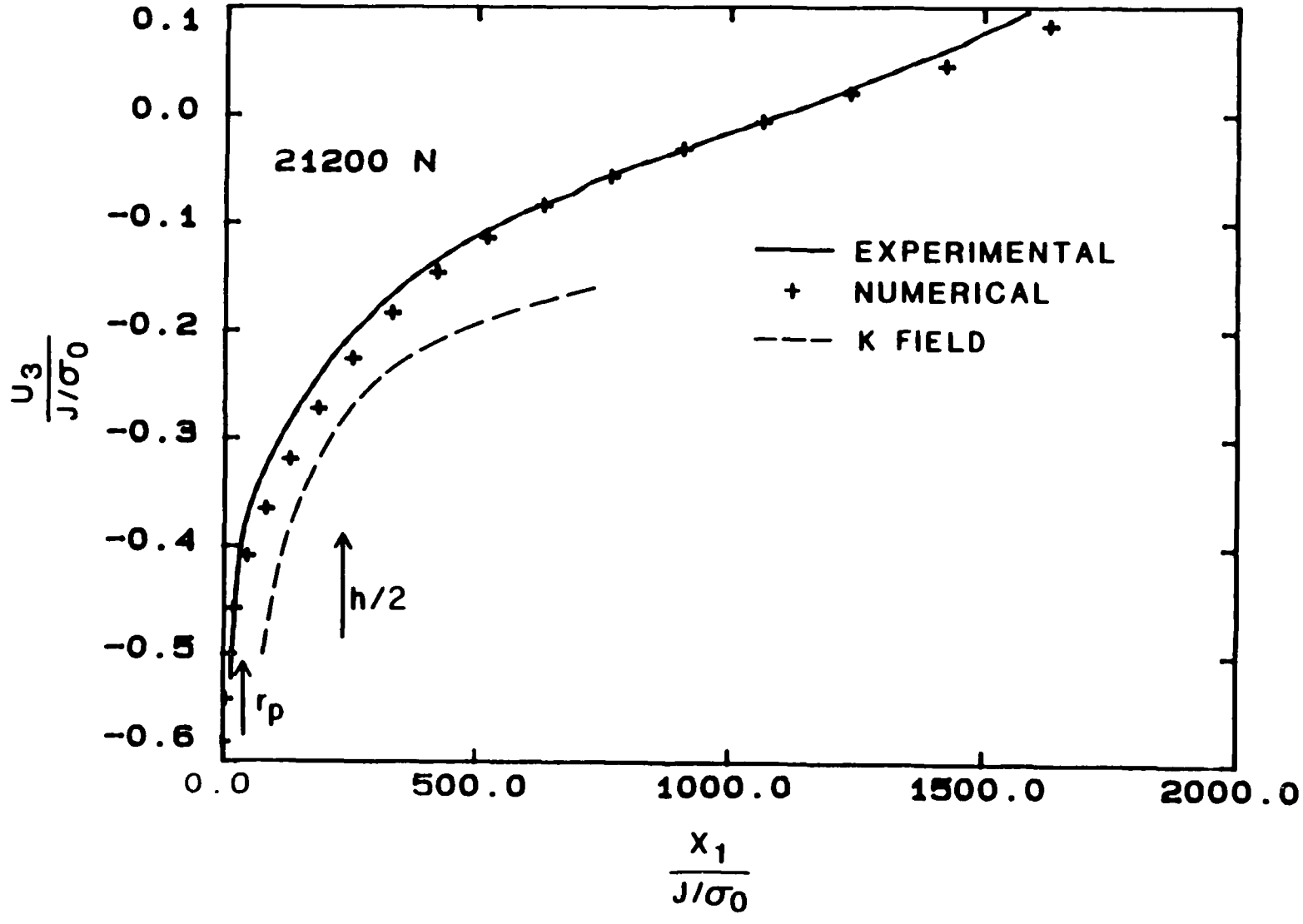

Figure 12.: Nondimensional u_3 displacement on the line $\theta = 0$. Comparison of experimental and numerical results for 21,200 N. Also shown is plane stress K_I field.

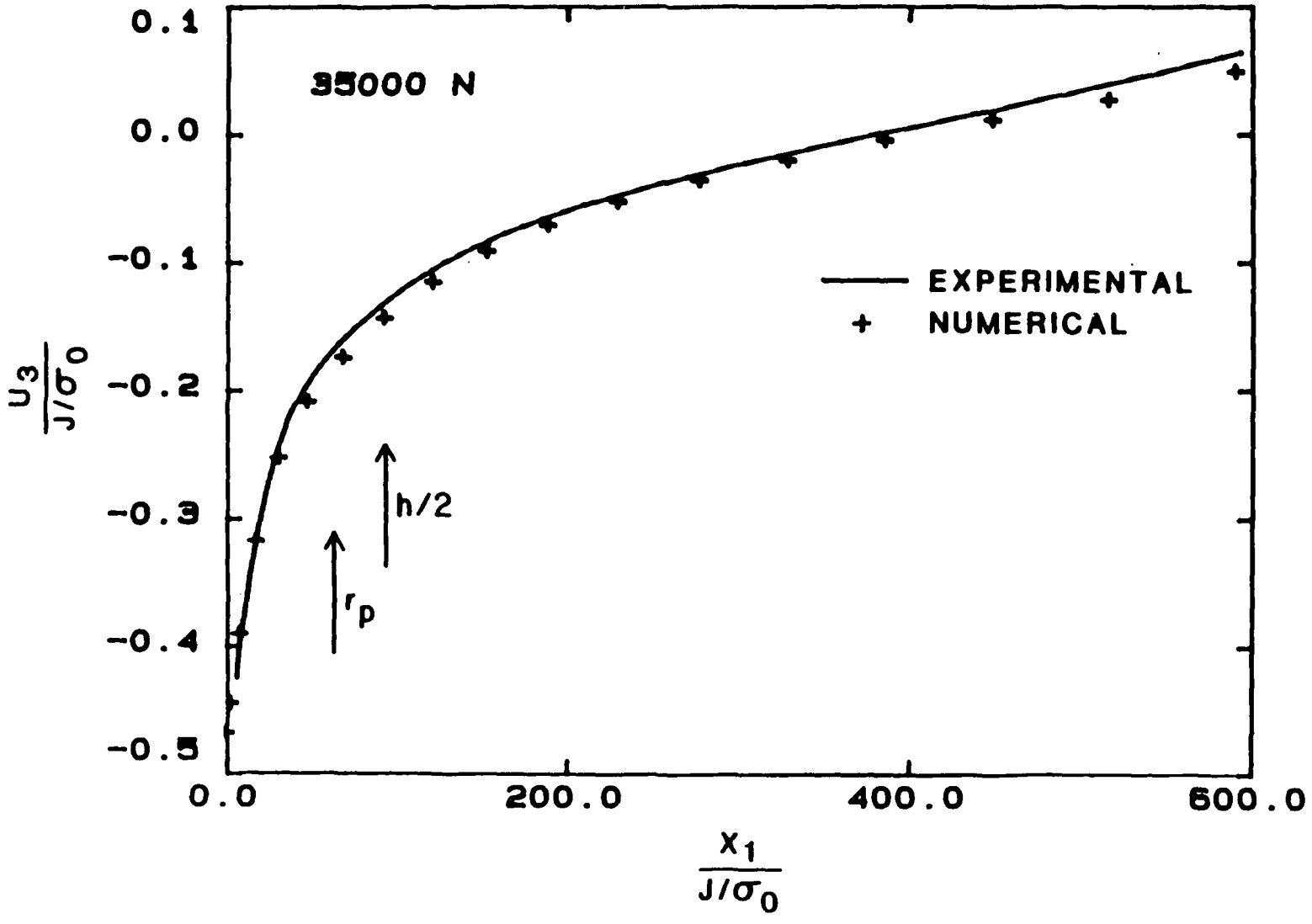

Figure 13.: Nondimensional u_3 displacement on the line $\theta = 0$. Comparison of experimental and numerical results for 35,000 N. Also shown is plane stress K_I field.

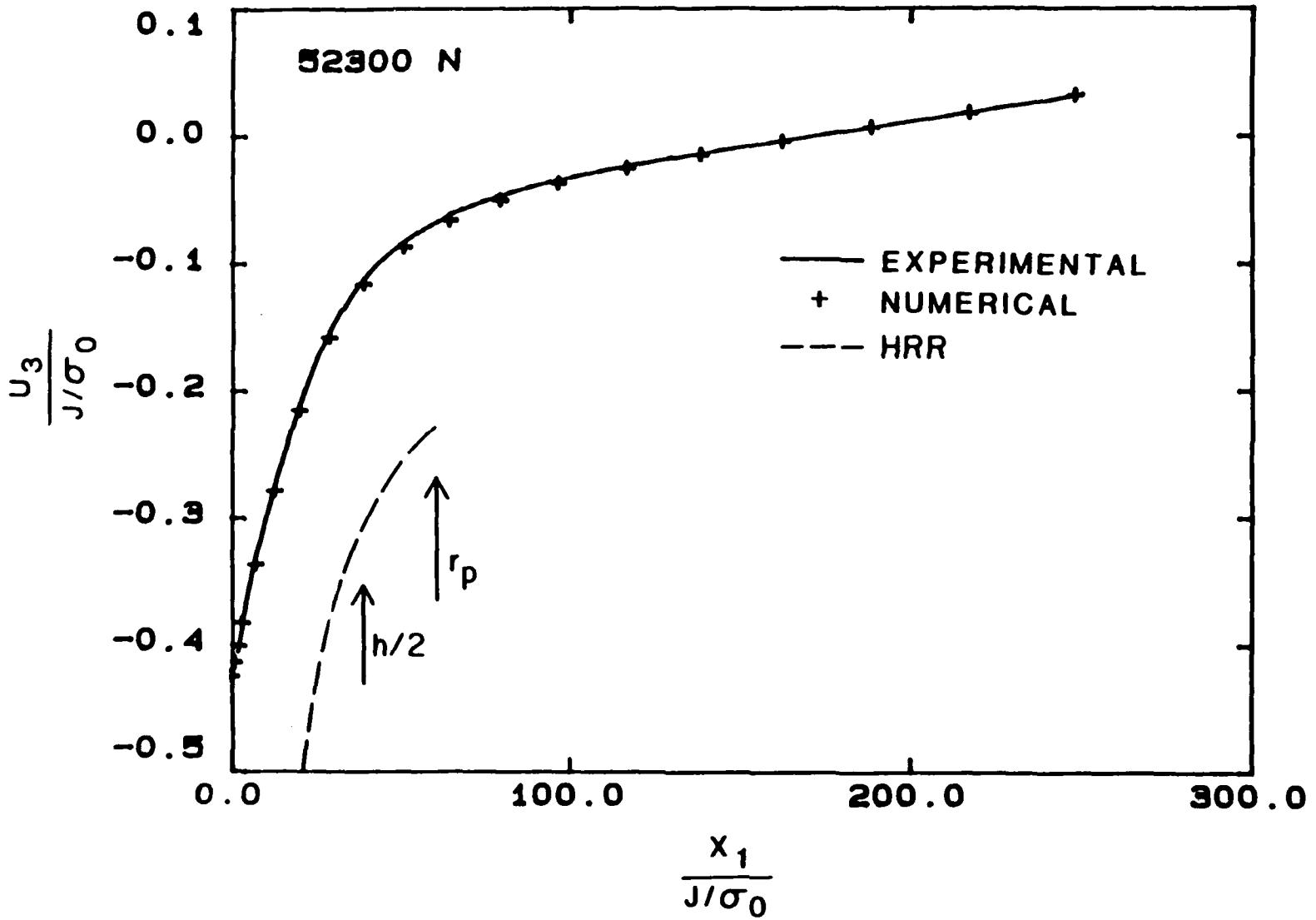

Figure 14.: Nondimensional u_3 displacement on the line $\theta = 0$. Comparison of experimental and numerical results for 52,300 N. Also shown is plane stress K_I field and u_3 from plane stress HRR field.

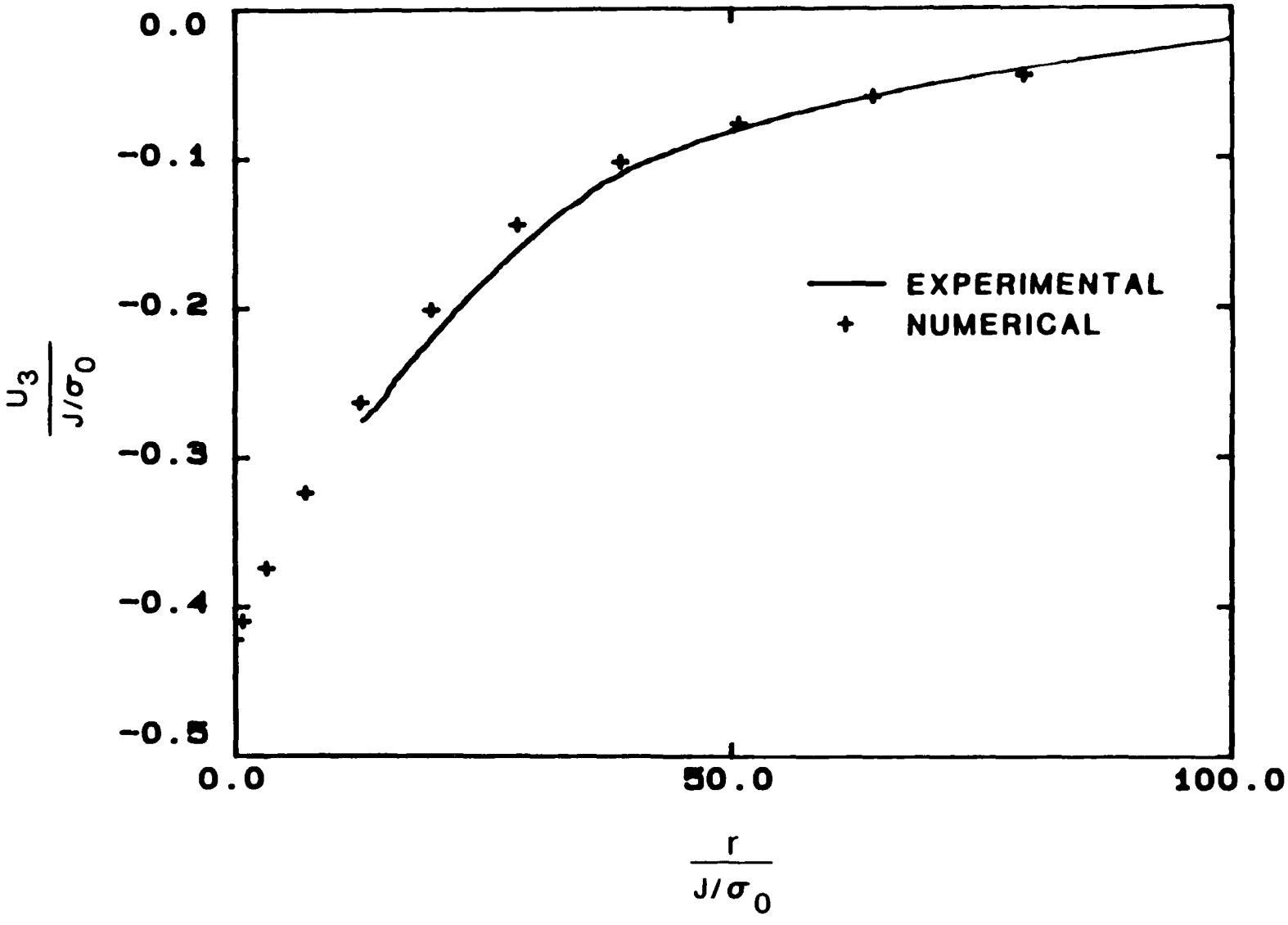

Figure 15.: Nondimensional u_3 displacement on the line $\theta = 40°$. Comparison of experimental and numerical results for 52,300 N.

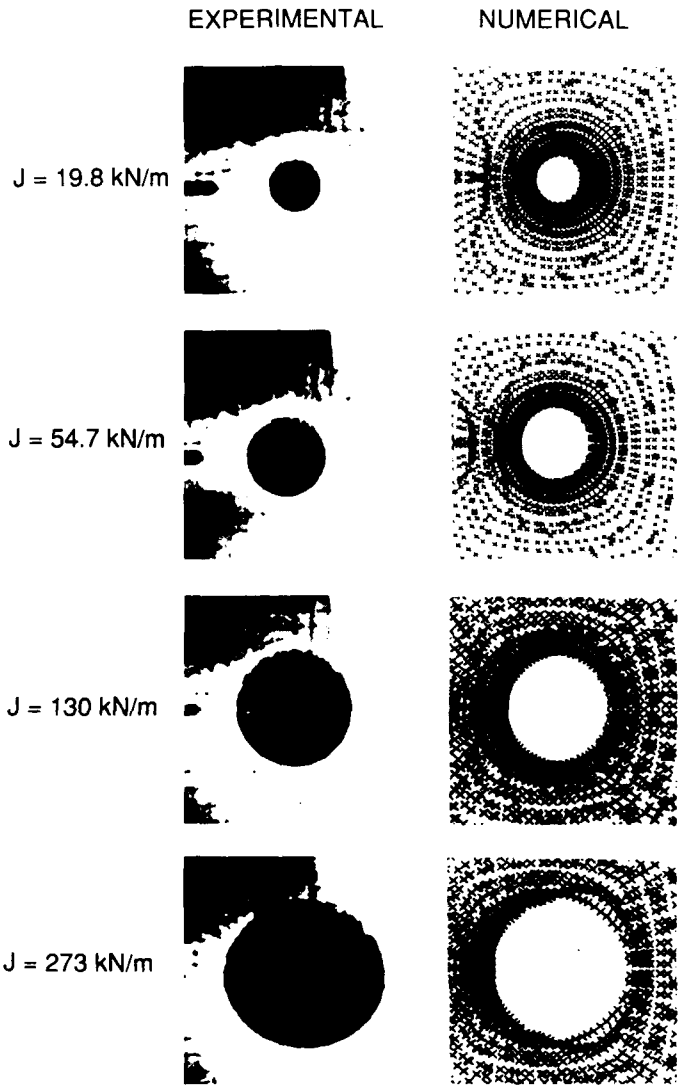

Figure 16.: Sequence of caustics for increasing loads, z_0 = 100 cm. Experimental results from specimen 67. Numerical results for 3-D numerical analysis.

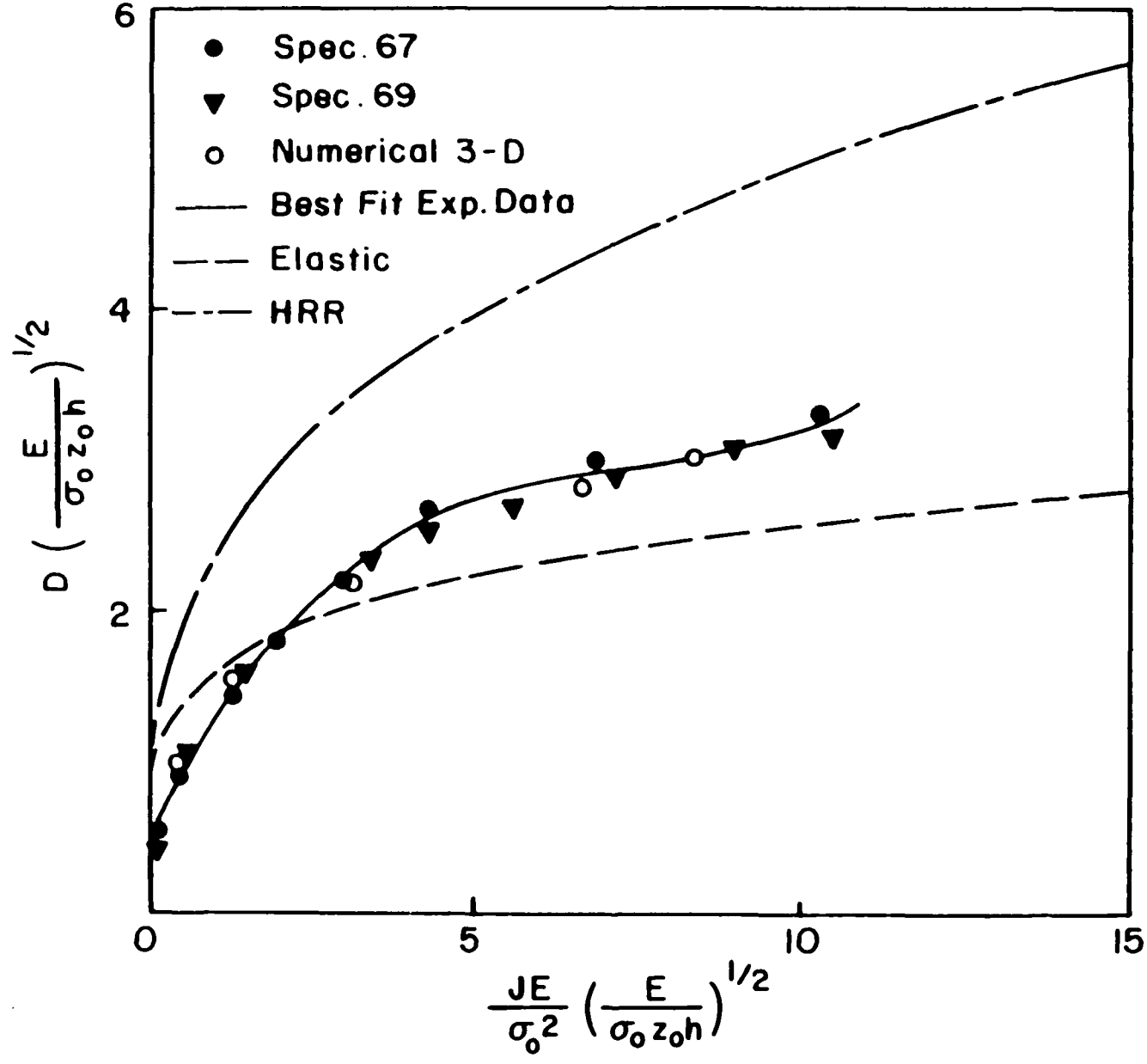

Figure 17.: Relation between caustic diameter D and J integral. Experimental and 3-D numerical results are shown. Also shown are relations from 2-D asymptotic analyses.

SECURITY CLASSIFICATION OF THIS PAGE (When Data Entered)

REPORT DOCUMENTATION PAGE

READ INSTRUCTIONS BEFORE COMPLETING FORM

1. REPORT NUMBER: SM 88-7
2. GOVT ACCESSION NO.:
3. RECIPIENT'S CATALOG NUMBER:

4. TITLE (and Subtitle): Three Dimensional Effects near a Crack Tip in a Ductile Three Point Bend Specimen Part II: An Experimental Investigation Using Interferometry and Caustics.

5. TYPE OF REPORT & PERIOD COVERED:

6. PERFORMING ORG. REPORT NUMBER:

7. AUTHOR(s): Alan T. Zehnder and Ares J. Rosakis

8. CONTRACT OR GRANT NUMBER(s): ONR Contract N00014-85-K-0596

9. PERFORMING ORGANIZATION NAME AND ADDRESS: Graduate Aeronautical Laboratories, 105-50 California Institute of Technology Pasadena, CA 91125

10. PROGRAM ELEMENT, PROJECT, TASK AREA & WORK UNIT NUMBERS:

11. CONTROLLING OFFICE NAME AND ADDRESS: Dr. Yapa Rajapakse, Program Manager ONR, Code 1132SM 800 N. Quincy St., Arlington, VA 22217-5000

12. REPORT DATE: January 1988

13. NUMBER OF PAGES: 20

14. MONITORING AGENCY NAME & ADDRESS(if different from Controlling Office):

15. SECURITY CLASS. (of this report): Unclassified

15a. DECLASSIFICATION/DOWNGRADING SCHEDULE:

16. DISTRIBUTION STATEMENT (of this Report):

17. DISTRIBUTION STATEMENT (of the abstract entered in Block 20, if different from Report):

18. SUPPLEMENTARY NOTES: Submitted for publication in Journal of Applied Mechanics

19. KEY WORDS (Continue on reverse side if necessary and identify by block number): Elastic-Plastic fracture, three dimensions, optical techniques, interferometry, caustics

20. ABSTRACT (Continue on reverse side if necessary and identify by block number):

An experimental investigation is undertaken to assess three-dimensional effects near a crack front in a ductile three-point bend specimen. The possibility of using the optical methods of caustics by reflection and Twyman-Green interferometry are performed simultaneously on either side of the test specimen. The load and load-point displacement are also measured. The experimental results are compared with very good agreement to the results of a finite element simulation of the experiment. The

DD FORM 1 JAN 73 1473 EDITION OF 1 NOV 65 IS OBSOLETE

S/N 0102-LF-014-6601

SECURITY CLASSIFICATION OF THIS PAGE (When Data Entered)

caustics experiments are used to obtain a calibration relation between the value of the J integral and the caustic diameter for load levels up to fracture initiation. It is proposed that such a calibration be used in dynamic fracture initiation experiments for the measurement of the time history of the dynamic J-integral.